Karlsruhe Institute of Technology

wave phenomena
analysis and numerics

A discrete Saint-Venant principle for finite element discretizations of elliptic problems

Tim Buchholz, Julian Dörner

CRC Preprint 2026/14, April 2026

KARLSRUHE INSTITUTE OF TECHNOLOGY

CRC 1173

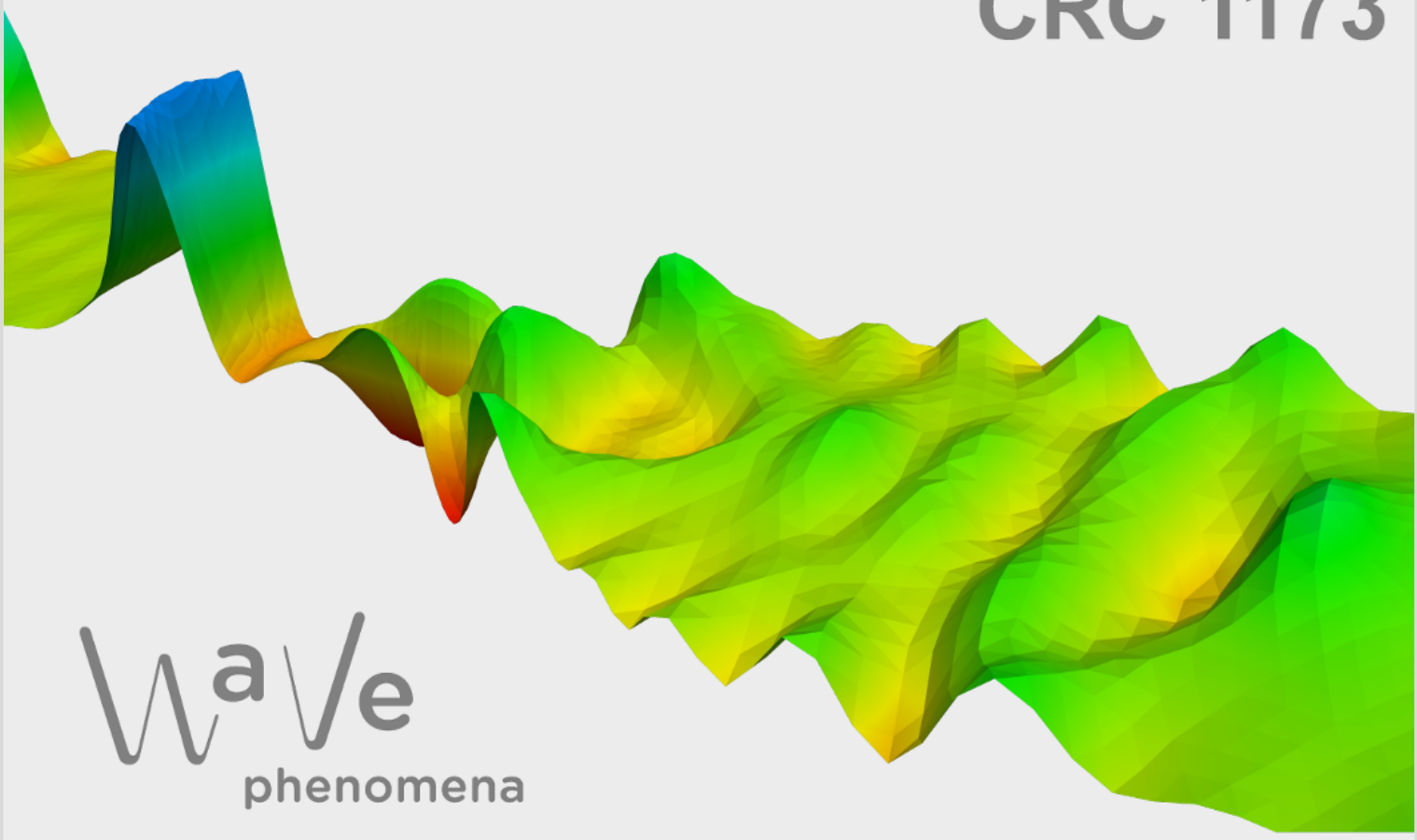

Participating universities

Funded by

ISSN 2365-662X

A DISCRETE SAINT-VENANT PRINCIPLE FOR FINITE ELEMENT DISCRETIZATIONS OF ELLIPTIC PROBLEMS

TIM BUCHHOLZ AND JULIAN DÖRNER

ABSTRACT. The present paper studies finite element discretizations of second-order elliptic boundary value problems with homogeneous right-hand side and inhomogeneous boundary conditions. We establish discrete spatial decay estimates on element patches for the energy norm of the discrete solution, showing that the influence of boundary data decays exponentially away from the boundary. The resulting estimates are a discrete analog of Saint-Venant-type principles and provide a rigorous foundation for localization arguments in finite element methods. As an application, we present how these results can be employed in the convergence analysis of domain decomposition methods, on the example of the discrete parallel Schwarz method. Finally, the findings are thoroughly demonstrated on several numerical examples.

1. INTRODUCTION

The spatial decay of boundary-induced effects in elliptic problems can be traced back to the Saint-Venant principle, originally formulated in the context of linear elasticity in the mid-19th century [34]. A classical and widely cited description states that *'...the difference between the effects of two different but statically equivalent loads becomes very small at sufficiently large distances from the load'*, cf. [28]. Early rigorous investigations focused on linear elasticity and established decay properties of stresses and strains away from regions of load application, see, e.g., [25,37].

It was soon recognized that the underlying mechanism is not specific to elasticity but rather a consequence of ellipticity. This insight led to extensions of Saint-Venant-type results to general second-order elliptic equations, where spatial decay of solutions was established primarily in a pointwise sense and under strong regularity assumptions, cf. [23,24,38]. Among these developments, the work of Mieth [32,33] is particularly relevant for the present paper, as it derives a decay estimate at the level of the energy norm. Since our analysis focuses on energy quantities, this perspective is the important analytical motivation of our work. Thus, we repeat the argument in brief below, see Section 1.1.

Comprehensive perspectives on the Saint-Venant principle and its extensions were later provided in a series of review articles by Horgan [20–22], emphasizing both the physical origins and the mathematical structure of the principle. While these classical results are formulated at the continuous level, they establish the conceptual foundation for spatial energy decay as a generic feature of elliptic operators.

In the present work, we adopt this viewpoint and investigate analogous decay phenomena directly at the discrete level. Our results may thus be interpreted as a finite element analogue of Saint-Venant-type principles, providing quantitative spatial energy decay estimates for discretizations of elliptic problems with homogeneous right-hand side and inhomogeneous boundary conditions.

2020 *Mathematics Subject Classification.* Primary 65N30, 65N22 Secondary 35J15, 65N55 .

Key words and phrases. finite element methods, Saint-Venant principle, elliptic boundary value problems, localization.

Spatial decay properties play a central—though often implicit—role in the analysis of domain decomposition (DD) methods; see, e.g., [12, 14, 36]. While many modern DD approaches are formulated at the matrix level, their analysis is frequently guided by continuous decay arguments, as discussed in detail in [12]. In particular, superlinear convergence results for Schwarz waveform relaxation methods rely on analytic decay properties of solutions to elliptic problems on unbounded or semi-infinite domains, cf. [11, 16].

Recent developments in DD methods for time-harmonic wave propagation have been made; see [7]. The authors formulate the problem on the skeleton of the subdivided domain and define exchange operators that govern the communication between subdomains. Many possible choices of such exchange operators are studied in [7, Sec. 5]. A particularly interesting choice for our work is a global exchange operator, which exhibits excellent stability properties but appears at first glance to be incompatible with a fast algorithm. In [6], it is numerically demonstrated that a truncation of this operator is sufficient and enables fast evaluation. This operator fits in the class of problems studied below.

More recent surveys, including work on time-parallel methods for parabolic and hyperbolic problems, further underline the importance of decay phenomena in both theoretical and practical contexts [13]. Related localization arguments also arise in tent-pitching methods combined with implicit time discretizations (cf. [18]), where the causality constraints limiting the admissible height of space–time tents may be interpreted as reflecting a localized influence of boundary and interface data. Finally, similar energy-based decay statements appear in [10] and constitute one of the main analytical tools in our own recent work [4].

Decay estimates are most explicitly exploited in numerical homogenization and multiscale methods. In the context of the localized orthogonal decomposition (LOD), Malqvist and Peterseim [30] proved the essential decay of corrector functions via Caccioppoli-type inequalities, justifying the truncation of global correctors to local patches; see also [31]. Closely related principles appear in generalized finite element methods (GFEM) and multiscale GFEM variants [1, 29], while alternative decay arguments based on Green's functions have been explored in [17]. Decay estimates of a similar nature also underlie localization phenomena for eigenstates of Schrödinger operators, which are closely related to the exponential decay of the associated Green's functions, as shown in [2].

These works demonstrate that spatial energy decay is a fundamental structural property underlying many modern numerical methods. The present paper aims to strengthen this perspective by establishing such decay directly for finite element discretizations, following the arguments of the aforementioned analytical results. We prove a fully discrete Saint-Venant-type principle with explicit mesh- and problem-dependent constants and demonstrate that its asymptotic behavior agrees with the decay rate of the analytical solution. We demonstrate the results on an overlapping domain decomposition algorithm. Furthermore, we thoroughly validate our results numerically, verify the dependence of problem-dependent parameters on the decay rate, and demonstrate their asymptotic optimality.

Outline. The paper is organized as follows. We close this section below with the analytical motivation on a simple example. Section 2 introduces the model problem and its variational formulation, the conforming finite element discretization, and the definition of local energies on element patches. Following that, we state in Section 3 our main results, i.e., the discrete spatial decay estimate for the finite element approximation, and show that its asymptotic behavior agrees with that of the corresponding continuous solution. In Section 4, we build the necessary tools for the proofs of the main results in Section 5. Section 6 demonstrates how

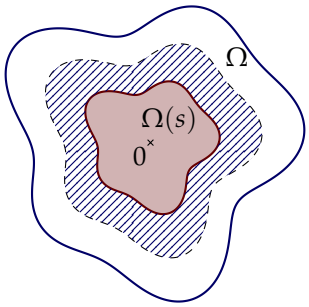

FIGURE 1. A smooth domain Ω, star shaped with respect to the origin. A subdomain $\Omega(s)$, for $s > 0$ is drawn in red, while the hatched blue area depicts $\Omega(s+\delta) \setminus \Omega(s)$.

the decay estimate can be used in the convergence analysis of an overlapping domain decomposition method. Finally, Section 7 presents numerical experiments that investigate the parameter dependence and asymptotic behavior predicted by the theory.

1.1. **Analytical motivation.** We briefly illustrate the proof technique on the continuous level to motivate our subsequent work. For simplicity, we choose a simplified setting which lags no descriptiveness and refer to the literature mentioned above for a more general setting; especially to the work from Mieth and Horgan, in particular [32, Chapter 2.3.1] and [22, Section II.D].

Let $\Omega \subset \mathbb{R}^2$ denote a smooth domain, star shaped with respect to the origin. The function $u \in C^2(\overline{\Omega})$ denotes the strong solution of the problem

$$-\Delta u + \lambda^2 u = 0 \ \text{ in } \Omega, \quad u = g \ \text{ on } \Gamma = \partial\Omega, \tag{1}$$

where g is a sufficiently smooth boundary datum. Centered around the origin, we define a series of subdomains of Ω as

$$\Omega(s) = \{\, sx \mid x \in \Omega \,\}, \quad 0 < s \leq 1 \qquad \Omega(1) = \Omega,$$

cf. Figure 1. We define the energy functional of the solution as $E(s) = \int_{\Omega(s)} |\nabla u|^2 + \lambda^2 u^2 \,\mathrm{d}x$ and prove the result

$$E(s) \leq e^{-2\lambda(1-s)} E(1), \quad \text{for } 0 < s \leq 1. \tag{2}$$

Hence, a smaller sub-domain has an exponentially smaller energy concentrated on it.

The proof follows two main steps, which we later replicate in the discrete setting. We first derive a differential inequality for the energy. By integration by parts, eq. (1), and Young's inequality, we obtain

$$E(s) = \int_{\Gamma(s)} u \nabla u \cdot n \,\mathrm{d}\sigma \leq \frac{1}{2\lambda} \int_{\Gamma(s)} |\nabla u|^2 + \lambda^2 u \,\mathrm{d}\sigma.$$

Integration of this inequality with $\delta = \frac{1}{2}(1-s)$ shows that

$$\int_s^{s+\delta} E(t) \,\mathrm{d}t \leq \frac{1}{2\lambda} \int_{\Omega(s+\delta)\setminus\Omega(s)} |\nabla u|^2 + \lambda^2 u \,\mathrm{d}\sigma = \frac{1}{2\lambda}(E(s+\delta) - E(s)).$$

Thus, we obtain the differential inequality

$$-\frac{\mathrm{d}}{\mathrm{d}s} \int_s^{s+\delta} E(t) \,\mathrm{d}t + 2\lambda \int_s^{s+\delta} E(t) \,\mathrm{d}t \leq 0.$$

In the next step, we solve the differential inequality and use monotonicity of the energy functional to obtain

$$\delta E(s) \leq \int_s^{s+\delta} E(t)\,\mathrm{d}t \leq e^{-2\lambda(1-s)} \int_{s+\delta}^1 E(t)\,\mathrm{d}t \leq \delta e^{-2\lambda(1-s)} E(1).$$

Division by δ then provides the desired result (2).

2. Preliminaries

2.1. **Sobolev spaces & traces.** In this section, we introduce the functional analytic framework. Let $\Omega \subset \mathbb{R}^d$ be a Lipschitz domain. Throughout the manuscript, we make use of the Lebesgue space $L^2(\Omega)$ of square integrable functions and denote its inner product and norm with $(\cdot,\cdot)_\Omega$ and $\|\cdot\|_{L^2(\Omega)}$, respectively.

We denote by $H^1(\Omega)$ the Sobolev space of functions with weak derivatives up to order one in $L^2(\Omega)$. The closure of the compactly supported test functions $C_c^\infty(\Omega)$ in $H^1(\Omega)$ is denoted by $H_0^1(\Omega)$. For the usual norm and semi-norm of $H^1(\Omega)$ we write $\|\cdot\|_{H^1(\Omega)}$ and $|\cdot|_{H^1(\Omega)}$, respectively.

It is well-known that every function $u \in H^1(\Omega)$ admits a well-defined trace $u\big|_{\partial\Omega} \in H^{1/2}(\partial\Omega)$, where the latter space denotes the fractional Sobolev space of order one half on the boundary $\partial\Omega$; see, for example, [8, Def. 2.14,Thm. 3.10]. In the model problem considered below, we will make use of functions that are only defined on a relatively open Lipschitz part of the boundary, i.e., $\Gamma \subset \partial\Omega$. Thus, we define the Lions-Magenes space as

$$H_{00}^{1/2}(\Gamma) = \{\, g \in H^{1/2}(\Gamma) \mid \widetilde{g} \in H^{1/2}(\partial\Omega) \,\}, \qquad \|g\|_{H_{00}^{1/2}(\Gamma)} = \|\widetilde{g}\|_{H^{1/2}(\partial\Omega)},$$

where $\widetilde{g}$ denotes the extension of g by zero to the whole of $\partial\Omega$. This space is alternatively defined via interpolation of Hilbert spaces, and we refer to [26] for a thorough treatment. Infamous for their abstractness, we emphasize that $H_0^{1/2+\epsilon}(\Gamma) \subset H_{00}^{1/2}(\Gamma)$ for any $\epsilon > 0$.

2.2. **Problem & variational formulation.** We now introduce the model problem. Let $\Omega \subset \mathbb{R}^d$ be a bounded and simply connected polyhedral domain. We denote with $\Gamma \subseteq \partial\Omega$ a simply connected subset of the boundary and define the complement $\Gamma^C = \partial\Omega \setminus \Gamma$. Let $\lambda \geq 0$ and $A \in L^\infty(\Omega, \mathbb{R}^{d\times d})$ be a positive and bounded coefficient that satisfies $\alpha \leq A(x) \leq \beta$ almost everywhere in Ω for positive constants $\alpha, \beta > 0$.

For a given $g \in H_{00}^{1/2}(\Gamma)$, we consider the following boundary value problem

$$\begin{aligned} -\nabla\cdot(A\nabla u) + \lambda^2 u &= 0, \quad \text{in } \Omega, \\ u\big|_\Gamma &= g, \quad \text{on } \Gamma, \\ u\big|_{\Gamma^C} &= 0, \quad \text{on } \Gamma^C. \end{aligned} \tag{3}$$

Recall that $\widetilde{g}$ is the extension of g by zero. As discussed in the previous section, we note that $\widetilde{g} \in H^{1/2}(\partial\Omega)$.

We emphasize that we allow in general $\Gamma = \partial\Omega$. Moreover, the case $\lambda = 0$ is permitted. However, to ensure coercivity of the problem, we restrict ourselves to the following two cases.

Assumption 2.1. *Either $\lambda > 0$ or $\Gamma^C \neq \emptyset$.*

In the following, we briefly discuss the well-posedness of (3). Since we have $\widetilde{g} \in H^{1/2}(\partial\Omega)$, we find a lifting $u_g \in H^1(\Omega)$ such that $u_g\big|_{\partial\Omega} = \widetilde{g}$ with

$$\|u_g\|_{H^1(\Omega)} \leq C_\gamma \|\widetilde{g}\|_{H^{1/2}(\partial\Omega)} = C_\gamma \|g\|_{H^{1/2}_{00}(\Gamma)}, \tag{4}$$

where $C_\gamma > 0$ is constant, uniform in g. We introduce the continuous bilinear form

$$\widehat{a}_\Omega : H^1(\Omega) \times H^1(\Omega) \to \mathbb{R}, \quad (u, v) \mapsto \int_\Omega (A\nabla u \cdot)\nabla v \,\mathrm{d}x,$$

and the restriction

$$a_\Omega = \widehat{a}_\Omega\big|_{H^1_0(\Omega)\times H^1_0(\Omega)}.$$

The bilinear form induces an equivalent semi-norm on $H^1(\Omega)$ defined as

$$|u|^2_{a,\Omega} = \widehat{a}_\Omega(u, u).$$

Thus, we define the natural energy norm of our problem as

$$|||u|||^2_\Omega = |u|^2_{a,\Omega} + \lambda^2 \|u\|^2_{L^2(\Omega)}. \tag{5}$$

The variational formulation of problem (3) reads: Seek $u \in H^1(\Omega)$ such that $u_0 = u - u_g \in H^1_0(\Omega)$ and

$$a_\Omega(u_0, v) + \lambda^2 (u_0, v)_\Omega = b(v), \quad \text{for all } v \in H^1_0(\Omega), \tag{6}$$

with the continuous linear form $b(v) = -\widehat{a}_\Omega(u_g, v) - \lambda^2(u_g, v)_\Omega$. Note that the left-hand side of (6) is coercive. The Lax-Milgram lemma, see [9, Lem. 25.2], thus shows that (6) is well-posed, and we obtain the *a priori* estimate $|||u_0|||_\Omega \leq |||u_g|||_\Omega$. Furthermore, we obtain the estimate for the solution

$$|||u|||_\Omega \leq 2\max\{\beta^{1/2}, \lambda\} \|u_g\|_{H^1(\Omega)} \leq 2C_\gamma \max\{\beta^{1/2}, \lambda\} \|g\|_{H^{1/2}_{00}(\Gamma)}. \tag{7}$$

2.3. **Space discretization by conforming finite elements.** Next, we discretize the variational problem by standard conforming Lagrange finite elements. We consider an affine, shape-regular, matching simplicial mesh $\mathcal{T}_h = \mathcal{T}_h(\Omega)$ of Ω, see, e.g., [8, Definition 8.11], where the parameter h denotes the maximal diameter of the elements in $\mathcal{T}_h$. We denote the minimal diameter of the elements in $\mathcal{T}_h$ by $h_{\min}$. Let $K \in \mathcal{T}_h$ be an element. We denote the set of all polynomials in d variables of degree $\leq k$ by $\mathbb{P}_k(K)$ for $k \geq 1$. Based on these sets of polynomials we introduce the finite-dimensional approximation space

$$\mathcal{P}_k(\mathcal{T}_h) \coloneqq \{v_h \in L^1(\Omega; \mathbb{R}) \quad | \quad v_h\big|_K \in \mathbb{P}_k(K),\ \forall K \in \mathcal{T}_h\} \cap C^0(\Omega; \mathbb{R}). \tag{8}$$

The subspace with homogenous boundary traces is denoted by $\mathcal{P}_{k,0}(\mathcal{T}_h)$.

Since the treatment of inhomogeneous boundary data is essential to our problem, we briefly recall it in the following and refer to [9] for more details. A finite element method is only able to produce solutions with boundary traces in the discrete trace space $\mathcal{P}_k(\mathcal{T}_h)\big|_{\partial\Omega}$. Therefore, the boundary data needs to be approximated, i.e., $g \approx g_h$ for a suitable $g_h \in \mathcal{P}_k(\mathcal{T}_h)\big|_{\partial\Omega}$. For the approximate g_h we choose, like in the continuos case, a lifting

$$u_{hg} \in \mathcal{P}_k(\mathcal{T}_h), \qquad \text{s.t. } u_{hg}\Big|_{\partial\Omega} = g_h. \tag{9}$$

The discretized analog of (6) then reads: Seek $u_h \in \mathcal{P}_k(\mathcal{T}_h)$ such that $u_{h0} = u_h - u_{hg} \in \mathcal{P}_{k,0}(\mathcal{T}_h)$ and

$$a_\Omega(u_{h0}, v_h) + \lambda^2 (u_{h0}, v_h)_\Omega = b_h(v_h), \quad \text{for all } v_h \in \mathcal{P}_{k,0}(\mathcal{T}_h), \tag{10}$$

where $b_h(v_h) = -\widehat{a}_\Omega(u_{hg}, v_h) - \lambda^2(u_{hg}, v_h)_\Omega$.

As in the continuous setting, coercivity ensures well-posedness via the Lax-Milgram lemma, and we obtain analogously to (4)

$$\|\!|u_h|\!\|_\Omega \leq 2\|\!|u_{hg}|\!\|_\Omega \leq 2\max\{\beta^{1/2},\lambda\}\|u_{hg}\|_{H^1(\Omega)}. \tag{11}$$

A particular choice of a lifting u_{hg} in (9) is a nodal one. We briefly recall its construction. For each element $K \in \mathcal{T}_h$, we introduce the nodal basis

$$\mathcal{N}_K := \{\sigma_{K,1},\dots,\sigma_{K,N_k^d}\}$$

consisting of the point evaluations $\sigma_{K,i}(v) = v(a_{K,i})$ at suitable nodal points $a_{K,i} \in K$ for $i = 1,\dots,N_k^d$, see e.g. [8, Section 7.4]. Hence, $(K, \mathbb{P}_k(K), \mathcal{N}_K)$ is the standard Lagrange finite element. We denote the set of all nodal points in $\mathcal{T}_h$ by $\mathcal{A}_h := \{a_1,\dots,a_{N_h}\}$ and corresponding global shape functions by φ_a for $a \in \mathcal{A}_h$, as in [8, Def. 19.2]. The set of nodal points on the boundary is defined as $\mathcal{A}_h^\partial = \{\, a \in \mathcal{A}_h \mid \varphi_a|_{\partial\Omega} \neq 0 \,\}$.

Let $g \in H_0^{s^*}(\Gamma)$, for $s^* > (d-1)/2$. This ensures that the embedding $H_0^s(\Gamma) \hookrightarrow C^0(\overline{\Gamma})$ is continuos, hence the pointwise evaluation of g is well-defined. Thus, the nodal approximation of $\widetilde{g}$ at the boundary is given by $g_h := \sum_{a\in\mathcal{A}_h^\partial} \widetilde{g}(a)\varphi_a|_{\partial\Omega}$, and the canonical lifting by

$$u_{hg} := \sum_{a\in\mathcal{A}_h^\partial} \widetilde{g}(a)\varphi_a \in \mathcal{P}_k(\mathcal{T}_h), \tag{12}$$

with the property that $u_{hg}|_{\partial\Omega} = g_h$.

While this nodal lifting is the natural choice for implementation, it is often desirable for analysis to introduce a discrete lifting that requires weaker regularity assumptions on g, and satisfies an estimate of the form (4). In Appendix A, we construct such a lifting, which is later used for the domain decomposition application in Section 6. Note, that the main results presented in Section 3 do not depend on the particular choice of the boundary lifting u_{hg}. This allows to pick the construction of u_{hg} dependent on the requirements driven by the application.

2.4. **Patches & patch energy.** In the following we introduce layered patches and associated energies. Let $D_h \subset \mathcal{T}_h$ be a fixed subset of elements. The set D_h is called *suitable* if $\Gamma \cap \overline{K} = \emptyset$ for all $K \in D_h$, hence D_h does not touch the inhomogeneous part of the boundary.

We define patches of elements around D_h recursively for $\ell \in \mathbb{N}$ by

$$\begin{aligned} P_0(D_h) &:= \{K \mid K \in D_h\} = D_h, \\ P_\ell(D_h) &:= \{K \in \mathcal{T}_h \mid \exists \widehat{K} \in P_{\ell-1}(D_h) \;:\; \overline{K} \cap \overline{\widehat{K}} \neq \emptyset\}. \end{aligned} \tag{13}$$

Patches are nested by definition, i.e., $P_\ell(D_h) \subset P_{\ell+1}(D_h)$. We call $P_\ell(D_h)$ the patch around D_h of size ℓ and define the maximal suitable patch size as

$$\ell_{\max} = \ell_{\max}(D_h) := \max\{\, \ell \in \mathbb{N} \mid \forall K \in P_\ell(D_h) :\; \overline{K} \cap \operatorname{supp} u_{hg} = \emptyset \,\}. \tag{14}$$

Thus, $\ell_{\max}$ is the maximal number of layers separating the set D_h from the support of the discrete lifting. For a nodal lifting, as described in (12), the support of u_{hg} consists of one boundary layer around Γ. Other discrete liftings might have a larger support, which we account for in (14). We refer to Figure 2 for an illustration of the construction.

Finally, the ℓ-th boundary layer of cells is denoted with

$$\Sigma_\ell(D_h) := P_\ell(D_h) \setminus P_{\ell-1}(D_h). \tag{15}$$

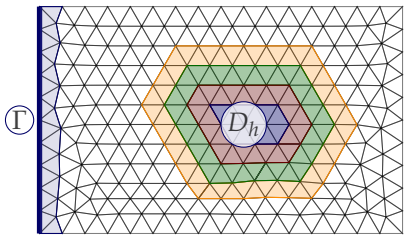

FIGURE 2. First three patches $P_\ell(D_h)$ for $\ell = 1$ (red), $\ell = 2$ (green) and $\ell = 3$ (orange). The support of nodal lifting u_{hg} (12) around Γ is depicted in light-blue, and $\ell_{\max} = 7$.

Let $u_h = u_{h0} + u_{hg} \in \mathcal{P}_k(\mathcal{T}_h)$ such that $u_{h0} \in \mathcal{P}_{k,0}(\mathcal{T}_h)$ solves the discrete problem (10). For any $\ell \in \mathbb{N}$ we define the *discrete energy in a patch around* D_h by

$$E_{D_h}(\ell) := \sum_{K \in P_\ell(D_h)} \int_K A\nabla u_h \cdot \nabla u_h \,\mathrm{d}x + \lambda^2 \int_K u_h u_h \,\mathrm{d}x. \tag{16}$$

This quantity is the discrete counterpart of the continuous energy functional introduced in Section 1.1 and will be the central object in the discrete Saint-Venant estimate.

3. MAIN RESULTS

We are now in a position to state the main result of this work. It establishes a discrete Saint-Venant-type principle for conforming finite elements. More precisely, we show that the discrete energy contained in successive element patches around a suitable interior cell set contracts by a factor strictly smaller than one. This layer-wise contraction implies exponential decay of the discrete energy with respect to the number of mesh layers separating the patch from the inhomogeneous boundary.

Theorem 3.1. *Let Assumption 2.1 hold and* $0 \le \ell < \ell_{max}$.
a) If $\lambda > 0$, *then*

$$E_{D_h}(\ell) \le \frac{M_\lambda}{1+M_\lambda} E_{D_h}(\ell+1) \quad \textit{with} \quad M_\lambda = C_1\big(1 + \frac{1}{2\lambda h_{\min}}\big). \tag{17}$$

b) If $\lambda = 0$, *then*

$$E_{D_h}(\ell) \le \frac{M_0}{1+M_0} E_{D_h}(\ell+1) \quad \textit{with} \quad M_0 = C_2\big(1 + \frac{1}{h_{\min}}\big). \tag{18}$$

The constants $C_1, C_2 > 0$ *only depend on the bounds of the material coefficient* α, β, *and the shape-regularity of the mesh but are uniform in the mesh size and* λ.

The proof of Theorem 3.1 will be presented in Section 5.

Corollary 3.2. *Let* $D_h \subset \mathcal{T}_h$ *be a suitable subset of elements. Then*

$$E_{D_h}(\ell) \le \rho E_{D_h}(\ell+1), \quad 0 \le \ell < \ell_{max}, \tag{19}$$

with $\rho < 1$ *depending on the regularity of the mesh, on the material parameters* α *and* β, *and also* λ *and the minimal element size* $h_{\min}$. *Moreover, we obtain*

$$E_{D_h}(0) \le \rho^{\ell_{max}} E_{D_h}(\ell_{max}) \le \rho^{\ell_{max}} |||u_h|||_\Omega^2 . \tag{20}$$

In words this means: The more layers of cells we can form between D_h and the support of u_{hg}, the smaller the discrete energy in D_h. The scaling is exponential in the number of layers $\ell_{\max}$.

Proof of Cor. 3.2. Following Theorem 3.1 the contraction factor ρ in (19) is given by

$$\rho = \frac{M}{1+M} < 1,$$

with $M = M_\lambda$ for $\lambda > 0$ and $M = M_0$ for $\lambda = 0$ defined in (17) and (18), respectively. To obtain (20) we apply Theorem 3.1 $\ell_{\max}$ times and then use (11). □

Next, we show that our decay rates agree with the expected analytic decay rate in the limit $h \to 0^+$. In that sense, we show that the discrete contraction factor obtained above is asymptotically consistent with the classical continuous decay rate as the mesh is refined. In particular, under quasi-uniform refinement, the discrete layer-wise decay converges to an exponential decay in the physical distance to the boundary.

Corollary 3.3. *Let the assumptions of Theorem 3.1 hold. Assume that the mesh sequence is quasi-uniform, i.e., $h_{\min}/h \to \theta \in (0,1]$, for $h \to 0^+$.*

a) If $\lambda > 0$, then

$$\Big(\frac{M_\lambda}{1+M_\lambda}\Big)^{1/h} \to \exp\Big(-\frac{2\lambda\theta}{C_1}\Big), \qquad h \to 0^+. \tag{21}$$

b) If $\lambda = 0$, then

$$\Big(\frac{M_0}{1+M_0}\Big)^{1/h} \to \exp\Big(-\frac{\theta}{C_2}\Big), \qquad h \to 0^+. \tag{22}$$

Proof of Cor. 3.3. Let $\rho = \frac{M_\lambda}{1+M_\lambda}$. We only prove a) since b) follows analogously with different coefficients. We determine the leading $h_{\min}$-coefficient of the map $h_{\min} \mapsto 1-\rho$ as

$$1-\rho = \frac{2\lambda h_{\min}}{C_1}\frac{1}{1+2\lambda(C_1^{-1}+1)h_{\min}}.$$

Therefore,

$$\frac{1}{h_{\min}}(1-\rho) \to \frac{2\lambda}{C_1}, \quad \text{for} \quad h_{\min} \to 0^+,$$

where we used the expansion $(1+\alpha h_{\min})^{-1} = 1 + \mathcal{O}(h_{\min})$, $h_{\min} \to 0^+$, for any $\alpha > 0$ in the second term. Thus, the expansion yields

$$\rho = 1 - \frac{2\lambda h_{\min}}{C_1} + \mathcal{O}(h_{\min}^2), \qquad h_{\min} \to 0^+.$$

With the expansion $\ln(1+x) = x + \mathcal{O}(x^2)$, for $|x| \to 0$, we obtain

$$\ln(\rho^{1/h_{\min}}) = \frac{1}{h_{\min}}\ln(\rho) = -\frac{2\lambda}{C_1} + \mathcal{O}(h_{\min}) \to -\frac{2\lambda}{C_1}, \qquad h_{\min} \to 0^+.$$

Finally, the claim is a result of the quasi-uniformity. □

Remark 3.4 (Geometric interpretation)**.** Corollary 3.3 allows for a qualitative geometric interpretation. Given an initial patch D_h with distance $\delta = \inf_{x\in D_h} \operatorname{dist}(x,\Gamma)$ to the boundary, the maximal number of possible layers (14) increases with the mesh size in the limit $h \to 0^+$, i.e., $\ell_{\max} \sim \delta/h$. Figure 3 illustrates this relation between mesh layers and geometric distance. Hence, we obtain with Corollaries 3.2 and 3.3 in the limit the estimate

$$E_{D_h}(0) \lesssim \rho^{\ell_{\max}} E_{D_h}(\ell_{\max}) \lesssim e^{-c\delta}\|g\|^2_{H^{s*}(\Gamma)},$$

where $c = 2\theta\lambda/C_1$ for $\lambda > 0$, and $c = \theta/C_2$ for $\lambda = 0$, respectively. Thus, the energy norm of the solution decays exponentially in the distance of the patch to the boundary. This is precisely a discrete version of the underlying analytic principle.

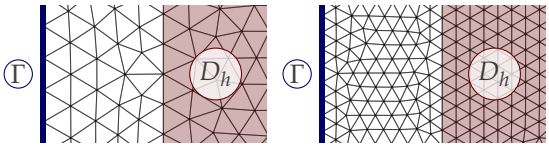

FIGURE 3. An interior set D_h (red) is separated from the inhomogeneous boundary Γ (blue) by several layers of mesh elements (white). Left: coarse mesh with relatively few admissible layers. Right: refined mesh with smaller mesh size h, allowing more layers between D_h and Γ. For fixed geometric distance $\delta = \inf_{x \in D_h} \operatorname{dist}(x, \Gamma)$, the number of layers scales as $\ell_{\max} \sim \delta / h$.

4. SMOOTH CUTOFF ON PATCHES

To evaluate the discrete energy locally on patches, we need a mechanism that allows us to restrict the discrete solution to a given patch without leaving the finite element space. To this end, we multiply the solution with a suitable cutoff function and interpolate the resulting product back into $\mathcal{P}_k(\mathcal{T}_h)$. In order to use this construction in the analysis, we require stability of the nodal interpolation operator when applied to products of discrete functions. We therefore briefly recall the definition of the Lagrange interpolation operator and collect the stability property needed in the sequel.

4.1. **Nodal interpolation.** Recall from Section 2.3 the definition of the Lagrange element $\big(K, \mathbb{P}_k(K), \mathcal{N}_K\big)$. Let $v \in C(K, \mathbb{R})$. We define the local interpolant by

$$\mathcal{I}_K v = \sum_{i=1}^{N_k^d} \sigma_{K,i}(v) \varphi_{a_{K,i}} = \sum_{i=1}^{N_k^d} v(a_{K,i}) \varphi_{a_{K,i}},$$

where $\varphi_{a_{K,i}}$ denotes the local shape function associated with the nodal point $a_{K,i}$. We can then further retrieve the standard Lagrange nodal interpolation for $v \in C^0(\overline{\Omega})$ by

$$\big(\mathcal{I}_h v\big)\big|_K = \mathcal{I}_K v, \qquad \forall K \in \mathcal{T}_h. \tag{23}$$

Lemma 4.1. *Let $K \in \mathcal{T}_h$. For $m = 0, 1$ there exists a constant $c_{\mathcal{I}}$ uniform in K and h, s.t.*

$$|\mathcal{I}_h(\phi_h \psi_h)|_{H^m(K)} \leq c_{\mathcal{I}} \, |\phi_h \psi_h|_{H^m(K)},$$

for all $\phi_h, \psi_h \in \mathcal{P}_k(\mathcal{T}_h)$. The constant $c_{\mathcal{I}}$ depends on the polynomial degree k, the spatial dimension n and the shape regularity of the mesh $\mathcal{T}_h$.

Proof. Let $m = 0$ or $m = 1$ and $|\cdot|_{H^0} = \|\cdot\|_{L^2}$. The argument is carried out on the reference element $\widehat{K}$. The map

$$Id - \mathcal{I}_{\widehat{K}} : (\mathbb{P}_{2k}(\widehat{K}), |\cdot|_{H^m}) \to (\mathbb{P}_{2k}(\widehat{K}), |\cdot|_{H^m})$$

is linear and bounded since $\dim(\mathbb{P}_{2k}(\widehat{K})) < \infty$ and the constant functions are in the kernel of the operator. Thus, it holds for $\widehat{\phi}_h, \widehat{\psi}_h \in \mathbb{P}_k(\widehat{K})$

$$\big|\mathcal{I}_h(\widehat{\phi}_h \widehat{\psi}_h)\big|_{H^m(\widehat{K})} \leq \big|\mathcal{I}_h(\widehat{\phi}_h \widehat{\psi}_h) - \widehat{\phi}_h \widehat{\psi}_h\big|_{H^m(\widehat{K})} + \big|\widehat{\phi}_h \widehat{\psi}_h\big|_{H^m(\widehat{K})} \leq c_1 \, \big|\widehat{\phi}_h \widehat{\psi}_h\big|_{H^m(\widehat{K})},$$

where $c_1 > 0$ depends on k, the reference element and the nodal set. Let $F_K : \widehat{K} \to K$ with $F_K(\widehat{x}) = B_K \widehat{x} + b_K$ be the affine map from the reference element $\widehat{K}$ to the physical element K. For any $\phi_h, \psi_h \in \mathbb{P}_k(K)$, we define $p = \phi_h \psi_h$ and $\widehat{p} = p \circ F_K$.

With the usual transformation properties, see, e.g., [5, Theorem 3.1.2], we conclude that

$$\begin{aligned}|\mathcal{I}_h p|_{H^m(K)} &\leq c_2 \|B^{-1}\|^m |\det B|^{1/2} |\mathcal{I}_{\widehat{K}} \widehat{p}|_{H^m(\widehat{K})} \\ &\leq c_2 \|B^{-1}\|^m |\det B|^{1/2} c_1 |\widehat{p}|_{H^m(\widehat{K})} \\ &\leq c_1 c_2^2 \|B\|^m \|B^{-1}\|^m |p|_{H^m(K)} ,\end{aligned}$$

with a constant $c_2 > 0$ depending on the dimension and m. Furthermore, the product $\|B\|\|B^{-1}\|$ is bounded uniformly by the shape regularity, see, e.g., [5, Theorem 3.1.3]. This proves the claim. □

4.2. **Discrete cutoff.** Recall the definition of patches $P_\ell(D_h)$ in (13). Similar to [30, Definition 3.3] we define for each $P_\ell(D_h)$ a discrete cutoff function $\eta_\ell \in \mathcal{P}_k(\mathcal{T}_h)$ with

$$0 \leq \eta_\ell \leq 1, \qquad \text{on } \Omega, \tag{24a}$$

$$\eta_\ell = 0, \qquad \text{on } \overline{K} \text{ for } K \in \mathcal{T}_h \setminus P_{\ell+1}(D_h), \tag{24b}$$

$$\eta_\ell = 1, \qquad \text{on } \overline{K} \text{ for } K \in P_\ell(D_h), \tag{24c}$$

$$\|\nabla \eta_\ell\|_{L^\infty(\Omega)} \leq c_\eta h_{\min}^{-1} , \tag{24d}$$

with a constant $c_\eta > 1$ uniform in $h_{\min}$.

By combining this cutoff function with the element-wise nodal interpolation $\mathcal{I}_h$ defined in (23) we define the following discrete cutoff operator, which will play a crucial role in the proof of Theorem 3.1. We define

$$\chi_h^\ell : \mathcal{P}_k(\mathcal{T}_h) \to \mathcal{P}_k(\mathcal{T}_h), \quad v_h \mapsto \mathcal{I}_h(\eta_\ell v_h). \tag{25}$$

Next, we gather important properties of χ_h^ℓ in the following Lemma.

Lemma 4.2. *Let $v_h \in \mathcal{P}_k(\mathcal{T}_h)$. Then, it holds:*

a) In $K \in P_\ell(D_h)$,

$$\chi_h^\ell v_h\big|_K = v_h\big|_K .$$

b) In $K \in \mathcal{T}_h \setminus P_{\ell+1}(D_h)$,

$$\chi_h^\ell v_h\big|_K = 0 .$$

c) In $K \in \Sigma_{\ell+1}$,

$$\int_K v_h \chi_h^\ell v_h \,\mathrm{d}x \leq c_{\mathcal{I}} \|v_h\|_{L^2(K)}^2 .$$

d) In $K \in \Sigma_{\ell+1}$,

$$\int_K A \nabla v_h \cdot \nabla(\chi_h^\ell v_h) \,\mathrm{d}x \leq c_{\mathcal{I}} \beta^{1/2} \|v_h\|_{a,K} \left(c_\eta h_{\min}^{-1} \|v_h\|_{L^2(K)} + \tfrac{1}{\alpha^{1/2}} \|v_h\|_{a,K} \right) .$$

Proof. Let $K \in P_\ell(D_h)$. We have $\eta_\ell = 1$ on $\overline{K}$ by (24c). Since $v_h \in \mathcal{P}_k(\mathcal{T}_h)$ and (23) this yields

$$\chi_h^\ell v_h\big|_K = \mathcal{I}_h(\eta_\ell v_h)\big|_K = \mathcal{I}_K(v_h\big|_K) = v_h\big|_K ,$$

which shows Lemma 4.2a). Next, let $K \in \mathcal{T}_h \setminus P_{\ell+1}(D_h)$. Then we get

$$\chi_h^\ell v_h\big|_K = \mathcal{I}_h(\eta_\ell v_h)\big|_K = \mathcal{I}_K(0) = 0 ,$$

since $\eta_\ell = 0$ on $\overline{K}$ by (24b), so Lemma 4.2b) holds.

For the remaining part of the proof, let $K \in \Sigma_{\ell+1}$. Note, that

$$\int_K v_h(\chi_h^\ell v_h) \,\mathrm{d}x \leq \|v_h\|_{L^2(K)} \left\|\mathcal{I}_h(\eta_\ell v_h)\right\|_{L^2(K)} . \tag{26}$$

By Lemma 4.1 and (24a) we get

$$\left\|\mathcal{I}_h(\eta_\ell v_h)\right\|_{L^2(K)} \leq c_{\mathcal{I}} \left\|\eta_\ell v_h\right\|_{L^2(K)} \leq c_{\mathcal{I}} \left\|\eta_\ell\right\|_{L^\infty(K)} \left\|v_h\right\|_{L^2(K)} \leq c_{\mathcal{I}} \left\|v_h\right\|_{L^2(K)}.$$

Combining this with (26) shows Lemma 4.2c).

Similarly, using the bound on $\left\|\nabla \eta_\ell\right\|_{L^\infty(\Omega)}$ from (24d) and Lemma 4.1 we derive

$$\begin{aligned}\int_K A\nabla v_h \nabla(\chi_h^\ell v_h)\,\mathrm{d}x &\leq \left\|v_h\right\|_{a,K} \left\|\mathcal{I}_h(\eta_\ell v_h)\right\|_{a,K} \\ &\leq \beta^{1/2} \left\|v_h\right\|_{a,K} \left|\mathcal{I}_h(\eta_\ell v_h)\right|_{H^1(K)} \\ &\leq c_{\mathcal{I}} \beta^{1/2} \left\|v_h\right\|_{a,K} \left|\eta_\ell v_h\right|_{H^1(K)}.\end{aligned}$$

Further, by the product rule we have

$$\begin{aligned}\left|\eta_\ell v_h\right|_{H^1(K)} &\leq \left\|\nabla \eta_\ell\right\|_{L^\infty(K)} \left\|v_h\right\|_{L^2(K)} + \left\|\eta_\ell\right\|_{L^\infty(K)} \left\|\nabla v_h\right\|_{L^2(K)} \\ &\leq c_\eta h_{\min}^{-1} \left\|v_h\right\|_{L^2(K)} + \tfrac{1}{\alpha^{1/2}} \left\|v_h\right\|_{a,K},\end{aligned}$$

which concludes the proof. □

5. Proof of Theorem 3.1

This section contains the proof of Theorem 3.1. The argument is structured in two steps.

First, we show that the energy $E_{D_h}(\ell)$ on the patch $P_\ell(D_h)$ defined in (16) can be represented as a flux across the outer layer $\Sigma_{\ell+1}$. Second, we bound this flux by the difference between the energies on two consecutive patches, $P_{\ell+1}(D_h)$ and $P_\ell(D_h)$. Combining both steps yields a contraction estimate

$$E_{D_h}(\ell) \leq M\big(E_{D_h}(\ell+1) - E_{D_h}(\ell)\big), \tag{27}$$

where the constant $M > 0$ depends explicitly on the parameter λ, the minimal mesh size $h_{\min}$, the bounds on the material coefficient α, β, and the shape-regularity of the mesh. The proof tracks these dependencies throughout. We treat the cases $\lambda > 0$ and $\lambda = 0$ separately. Rearranging (27) then gives (17) and (18), respectively.

5.1. Strictly positive $\lambda > 0$.

Proof of Theorem 3.1a). Recall, that $u_{h0} = u_h - u_{hg} \in \mathcal{P}_{k,0}(\mathcal{T}_h)$ satisfies (10). By assumption it holds that $\ell < \ell_{\max}$, and the definition of $\ell_{\max}$ in (14) implies that $P_{\ell+1}(D_h) \cap \operatorname{supp} u_{hg} = \emptyset$. Therefore, the energy on $P_\ell(D_h)$ is the same for both u_h and u_{h0}, i.e., we define

$$E_{D_h,0}(\ell) \coloneqq \sum_{K \in P_\ell(D_h)} \int_K A\nabla u_{h0} \cdot \nabla u_{h0}\,\mathrm{d}x + \lambda^2 \int_K u_{h0} u_{h0}\,\mathrm{d}x = E_{D_h}(\ell). \tag{28}$$

Let χ_h^ℓ be defined as in (25). By Lemma 4.2a), it holds that $\chi_h^\ell u_{h0}\big|_K = u_{h0}$ for $K \in P_\ell(D_h)$. Thus, we can plug the cut-off function under the integral and obtain

$$E_{D_h,0}(\ell) = \sum_{K \in P_\ell(D_h)} \int_K A\nabla u_{h0} \cdot \nabla(\chi_h^\ell u_{h0})\,\mathrm{d}x + \lambda^2 \int_K u_{h0}(\chi_h^\ell u_{h0})\,\mathrm{d}x. \tag{29}$$

Again, by definition, the function $\chi_h^\ell u_{h0} \in \mathcal{P}_{k,0}(\mathcal{T}_h)$ is a valid test function for the variational formulation (10), and we see that

$$a_\Omega(u_{h0}, \chi_h^\ell u_{h0}) + \lambda^2 (u_{h0}, \chi_h^\ell u_{h0})_\Omega = b_h(\chi_h^\ell u_{h0}). \tag{30}$$

From $b_h(\chi_h^\ell u_{h0}) = -\widehat{a}_\Omega(u_{hg}, \chi_h^\ell u_{h0}) - \lambda^2 (u_{hg}, \chi_h^\ell u_{h0})_\Omega$ we conclude that

$$\operatorname{supp} \chi_h^\ell u_{h0} \cap \operatorname{supp} u_{hg} = \emptyset \implies b_h(\chi_h^\ell u_{h0}) = 0. \tag{31}$$

Hence, the right-hand side of (30) vanishes.

This allows for subtraction of (30) from (29), which yields together with Lemma 4.2b)

$$\begin{aligned} E_{D_h,0}(\ell) &= \sum_{K \in P_\ell(D_h)} \int_K A \nabla u_{h0} \cdot \nabla(\chi_h^\ell u_{h0}) \,\mathrm{d}x + \lambda^2 \int_K u_{h0} (\chi_h^\ell u_{h0}) \,\mathrm{d}x \\ &\quad - a_\Omega(u_{h0}, \chi_h^\ell u_{h0}) + \lambda^2 (u_{h0}, \chi_h^\ell u_{h0})_\Omega \\ &= \sum_{K \in P_\ell(D_h)} \int_K A \nabla u_{h0} \cdot \nabla(\chi_h^\ell u_{h0}) \,\mathrm{d}x + \lambda^2 \int_K u_{h0} (\chi_h^\ell u_{h0}) \,\mathrm{d}x \\ &\quad - \sum_{K \in \mathcal{T}_h} \int_K A \nabla u_{h0} \cdot \nabla(\chi_h^\ell u_{h0}) \,\mathrm{d}x + \lambda^2 \int_K u_{h0} (\chi_h^\ell u_{h0}) \,\mathrm{d}x \\ &= - \sum_{K \in \Sigma_{\ell+1}} \int_K A \nabla u_{h0} \cdot \nabla(\chi_h^\ell u_{h0}) \,\mathrm{d}x + \lambda^2 \int_K u_{h0} (\chi_h^\ell u_{h0}) \,\mathrm{d}x \,. \end{aligned} \tag{32}$$

By assumption (14), the lifting u_{hg} is unsupported in $\Sigma_{\ell+1}$, i.e., $\overline{K} \cap \operatorname{supp} u_{hg} = \emptyset$ for $K \in \Sigma_{\ell+1}$. Therefore, $u_h|_K = u_{h0}|_K$ for any $K \in \Sigma_{\ell+1}$, and the equality in (29) shows that

$$E_{D_h}(\ell) = E_{D_h,0}(\ell) = - \sum_{K \in \Sigma_{\ell+1}} \int_K A \nabla u_h \cdot \nabla(\chi_h^\ell u_h) \,\mathrm{d}x + \lambda^2 \int_K u_h (\chi_h^\ell u_h) \,\mathrm{d}x \,. \tag{33}$$

Using Lemma 4.2c) and Lemma 4.2d) we derive the estimate

$$E_{D_h}(\ell) \leq c_{\mathcal{I}} \sum_{K \in \Sigma_{\ell+1}} \Big(\lambda^2 \|u_h\|_{L^2(K)}^2 + \beta^{1/2} \|u_h\|_{a,K} \Big(c_\eta h_{\min}^{-1} \|u_h\|_{L^2(K)} + \tfrac{1}{\alpha^{1/2}} \|u_h\|_{a,K} \Big) \Big).$$

The occurring mixed term is estimated by Young's inequality

$$\sum_{K \in \Sigma_{\ell+1}} \|u_h\|_{a,K} \|u_h\|_{L^2(K)} \leq \frac{1}{2\lambda} \Big(\sum_{K \in \Sigma_{\ell+1}} \|u_h\|_{a,K}^2 + \lambda^2 \sum_{K \in \Sigma_{\ell+1}} \|u_h\|_{L^2(K)}^2 \Big), \tag{34}$$

which yields for $c_\eta > 1$

$$E_{D_h}(\ell) \leq c_{\mathcal{I}} \Big(\frac{\beta^{1/2}}{\alpha^{1/2}} + \frac{\beta^{1/2} c_\eta}{2\lambda h_{\min}} \Big) \Big(\sum_{K \in \Sigma_{\ell+1}} \|u_h\|_{a,K}^2 + \lambda^2 \sum_{K \in \Sigma_{\ell+1}} \|u_h\|_{L^2(K)}^2 \Big). \tag{35}$$

The right-hand side term in (37) is now the difference between the energies, i.e.,

$$\sum_{K \in \Sigma_{\ell+1}} \|u_h\|_{a,K}^2 + \lambda^2 \sum_{K \in \Sigma_{\ell+1}} \|u_h\|_{L^2(K)}^2 = E_{D_h}(\ell+1) - E_{D_h}(\ell). \tag{36}$$

Hence, this proves the claim

$$E_{D_h}(\ell) \leq C_1 \big(1 + \frac{1}{2\lambda h_{\min}}\big) \Big(E_{D_h}(\ell+1) - E_{D_h}(\ell) \Big), \tag{37}$$

where the constant $C_1 > 0$ depends on $c_{\mathcal{I}}, c_\eta, \alpha$, and β. □

5.2. **Vanishing $\lambda = 0$.** We proceed with the proof for the case $\lambda = 0$, which is similar to the previous one. Additionally, we require a Poincaré inequality, e.g. [3, Thm. 10.6.12].

Proof of Theorem 3.1b). We distinguish again two cases: First, let $\overline{K} \cap \Gamma^C = \emptyset$ for all $K \in P_\ell(D_h)$. Let $c \geq 0$ be a constant, which will be determined later. Since $\nabla c = 0$, we proceed as in the proof of Theorem 3.1 and obtain

$$E_{D_h,0} := \sum_{K \in P_\ell(D_h)} \int_K A \nabla u_{h0} \nabla (u_{h0} - c) \, \mathrm{d}x = E_{D_h}(\ell) \tag{38}$$

With Lemma 4.2a) it holds that

$$E_{D_h,0} = \sum_{K \in P_\ell(D_h)} \int_K A \nabla u_{h0} \nabla (\chi_h^\ell (u_{h0} - c)) \, \mathrm{d}x. \tag{39}$$

Since $\overline{K} \cap \partial\Omega = \emptyset$ for all $K \in P_\ell(D_h)$, the function $\chi_h^\ell(u_{h0} - c) \in \mathcal{P}_{k,0}(\mathcal{T}_h)$ is a valid test function and (10) shows that

$$a_\Omega\big(u_{h0}, \chi_h^\ell(u_{h0} - c)\big) = b_h\big(\chi_h^\ell(u_{h0} - c)\big) = 0. \tag{40}$$

The last equality is a consequence of $K \cap \operatorname{supp} u_{hg} = \emptyset$ for $K \in \Sigma_{\ell+1}$ since $\ell < \ell_{\max}$.

Taking the difference between (39) and (40) and repeating arguments above for (32) and (33) shows that

$$E_{D_h}(\ell) = -\sum_{K \in \Sigma_{\ell+1}} \int_K A \nabla u_h \nabla (\chi_h^\ell (u_h - c)) \, \mathrm{d}x. \tag{41}$$

Using Lemma 4.2d) and Young's inequality with $\gamma > 0$ shows that

$$E_{D_h}(\ell) \leq c_{\mathcal{I}} \beta^{1/2} \Big(\sum_{K \in \Sigma_{\ell+1}} \big(\frac{1}{\alpha^{1/2}} + \frac{c_\eta}{2\gamma h_{\min}} \big) \|u_h\|_{a,K}^2 + \frac{\gamma c_\eta}{2 h_{\min}} \int_{Z_{\ell+1}} |u_h - c|^2 \, \mathrm{d}x \Big), \tag{42}$$

where $Z_{\ell+1} = \operatorname{int}\big(\bigcup_{K \in \Sigma_{\ell+1}} \overline{K}\big)$. We choose $c = \int_{Z_{\ell+1}} u_h \, \mathrm{d}x$ and obtain with the Poincaré inequality, see for example [3, Thm. 10.6.12, eq. (10.6.13)], that

$$\int_{Z_{\ell+1}} |u_h - c|^2 \, \mathrm{d}x \leq C_{\mathrm{p}} \sum_{K \in \Sigma_{\ell+1}} |u_h|_{H^1(K)}^2 \leq \frac{C_{\mathrm{p}}}{\alpha} \sum_{K \in \Sigma_{\ell+1}} \|u_h\|_{a,K}^2, \tag{43}$$

with a constant $C_{\mathrm{p}} > 0$ that depends on the smallest angle of all elements K comprising $\Sigma_{\ell+1}$. Thus, from (42) we obtain

$$E_{D_h}(\ell) \leq c_{\mathcal{I}} \frac{\beta^{1/2}}{\alpha^{1/2}} \Big(1 + \frac{c_\eta \alpha^{1/2}}{2\gamma h_{\min}} + \frac{\gamma c_\eta C_{\mathrm{p}}}{2 h_{\min} \alpha^{1/2}} \Big) \sum_{K \in \Sigma_{\ell+1}} \|u_h\|_{a,K}^2,$$

which yields by choosing $\gamma = \big(\alpha / C_{\mathrm{p}}\big)^{1/2}$ and repeating the argument from above for (34)-(36)

$$E_{D_h}(\ell) \leq c_{\mathcal{I}} \frac{\beta^{1/2}}{\alpha^{1/2}} \Big(1 + \frac{c_\eta \sqrt{C_{\mathrm{p}}}}{h_{\min}} \Big) \big(E_{D_h}(\ell + 1) - E_{D_h}(\ell) \big). \tag{44}$$

The claim follows for this case directly with $C_2 = c_{\mathcal{I}} c_\eta \beta^{1/2} \alpha^{-1/2} \sqrt{C_{\mathrm{p}}}$.

In the second case, the patch $P_\ell(D_h)$ touches the homogeneous Dirichlet boundary, i.e., $\overline{K}_\star \cap \Gamma^C \neq \emptyset$ for some $K_\star \in P_\ell(K)$. Here, we set $c = 0$ in above derivation and replace (43) using [3, Thm. 10.6.12, eq. (10.6.14)] with

$$\|u_h\|_{L^2(Z_{\ell+1})}^2 \leq \frac{C_{\mathrm{p},0}}{\alpha} \sum_{K \in \Sigma_{\ell+1}} \|u_h\|_{a,K}^2, \tag{45}$$

where $C_{\mathrm{p},0}$ depends only on the shape regularity of $\Sigma_{\ell+1}$. The rest of the proof follows analogously with $C_2 = c_{\mathcal{I}} c_\eta \beta^{1/2} \alpha^{-1/2} \sqrt{C_{\mathrm{p},0}}$. □

Remark 5.1 (Localized right-hand sides)**.** The mechanism behind Theorem 3.1 relies on spatial separation between inhomogeneous data and the region where the energy is measured rather than on boundary conditions themselves. Consequently, analogous decay estimates hold for problems with homogeneous boundary conditions and spatially localized right-hand sides, since the discrete solution satisfies a homogeneous equation outside the support of the data.

This recovers exponential energy decay estimates used in localized orthogonal decomposition and related multiscale methods; see, e.g., [31, Theorem 4.1], [2, Corollary 3.7], and [10, Lemma 3.1]. Hence, boundary- and source-driven decay arise from the same locality property of the discrete elliptic operator.

Remark 5.2. While the construction of the discrete cutoff operator from Section 4 reminds of techniques used in the analysis of multiscale methods — in particular in the localization of corrector functions within the LOD framework, see for example [30] and [31, Chapter 4] — the present approach differs in a fundamental way. No multiscale decomposition or orthogonality property is invoked. Instead, the localization mechanism is applied directly to the full conforming finite element solution, while using the discrete product estimate of the nodal interpolation. From a conceptual point of view, the proof of Theorem 3.1 presented in Section 5 is closer to the classical energy-based decay arguments of Mieth and Horgan, translated to the discrete setting.

6. Application: Discrete Parallel Schwarz Method

The discrete decay estimate of Theorem 3.1 provides a natural tool for studying the propagation of interface information in iterative domain decomposition methods. In particular, it allows us to analyze the convergence of a parallel Schwarz iteration for a finite element discretization of an elliptic boundary value problem.

To this end, we consider the Laplace problem on a bounded polygonal domain $\Omega \subset \mathbb{R}^2$,

$$\begin{aligned} -\Delta u &= f, \quad \text{in } \Omega, \\ u &= 0, \quad \text{on } \partial\Omega. \end{aligned} \tag{46}$$

Rather than solving (46) directly on Ω, we introduce overlapping subdomains Ω_1 and Ω_2, together with their interfaces

$$\Gamma_i := \partial\Omega_i \cap \Omega, \qquad i = 1, 2.$$

We then solve iteratively, for $n \geq 0$,

$$\begin{aligned} -\Delta u^1_{n+1} &= f, && \text{in } \Omega_1, & -\Delta u^2_{n+1} &= f, && \text{in } \Omega_2, \\ u^1_{n+1} &= 0, && \text{on } \partial\Omega \cap \partial\Omega_1, & u^2_{n+1} &= 0, && \text{on } \partial\Omega \cap \partial\Omega_2, \\ u^1_{n+1} &= u^2_n, && \text{on } \Gamma_1, & u^2_{n+1} &= u^1_n, && \text{on } \Gamma_2. \end{aligned} \tag{47}$$

This iterative scheme is known as the parallel Schwarz method and dates back to [27]. As described in (47), the method is typically formulated at the continuous level, although it is ultimately combined with a spatial discretization.

The convergence analysis of this method, as well as of many related domain decomposition schemes, is often carried out either continuously in space, that is, prior to the application of a spatial discretization (see, e.g., [14, Section 2]), or after discretization, at the matrix level (see, e.g., [36, Chapter 2]). In contrast, Theorem 3.1 provides another approach to proving the convergence of a finite element discretization of (47), which incorporates the spatial discretization directly.

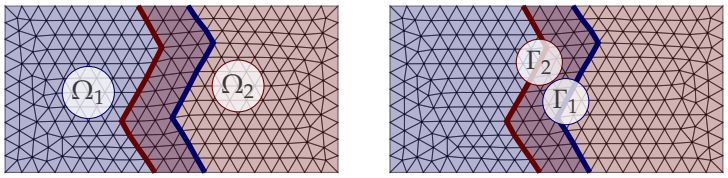

FIGURE 4. Left: Example decomposition of a rectangular domain into two overlapping subdomains Ω_1 and Ω_2 with $\ell_{\mathrm{ov}} = 3$. Right: Interfaces Γ_1 and Γ_2 of the subdomains.

For simplicity, we consider a rectangular domain Ω with two fixed overlapping subdomains Ω_1 and Ω_2, and denote by ℓ_{ov} the number of mesh layers in the overlap; see Figure 4 for an illustration.

The finite element discretization of (47) then iteratively seeks a sequence of solutions

$$\left(u^1_{h,n}, u^2_{h,n}\right) \in \mathcal{P}_k(\mathcal{T}_h(\Omega_1)) \times \mathcal{P}_k(\mathcal{T}_h(\Omega_2)), \qquad n \geq 0, \tag{48a}$$

solving the two problems

$$\begin{aligned} a_{\Omega_1}(u^1_{h,n+1}, \varphi^1_h) &= \left(f, \varphi^1_h\right)_{\Omega_1}, \quad \text{for all } \varphi^1_h \in \mathcal{P}_{k,0}(\mathcal{T}_h(\Omega_1)) \\ u^1_{h,n+1}\Big|_{\Gamma_1} &= u^2_{h,n}\Big|_{\Gamma_1}, \\ a_{\Omega_2}(u^2_{h,n+1}, \varphi^2_h) &= \left(f, \varphi^2_h\right)_{\Omega_2}, \quad \text{for all } \varphi^1_h \in \mathcal{P}_{k,0}(\mathcal{T}_h(\Omega_2)) \\ u^2_{h,n+1}\Big|_{\Gamma_2} &= u^1_{h,n}\Big|_{\Gamma_2}, \end{aligned} \tag{48b}$$

with some initial values $u^1_{h,0}$ and $u^2_{h,0}$. Note, that we do not rely on any specific lifting of the boundary datum. The usual nodal lifting is sufficient and preferred for implementation.

We aim to prove that our iteration is a contraction when compared to a global discretization of (46). Hence, we define $u_h \in \mathcal{P}_{k,0}(\mathcal{T}_h)$ as the solution of

$$a_\Omega(u_h, \varphi_h) = \left(f, \varphi_h\right)_\Omega, \qquad \text{for all } \varphi_h \in \mathcal{P}_{k,0}(\mathcal{T}_h). \tag{49}$$

The discrete error of the n-th iterates is now defined as

$$\mathcal{E}_{h,n} := \sum_{i=1,2} \left\|u^i_{h,n} - u_h\right\|^2_{a,\Omega_i} = \sum_{i=1,2} \left|u^i_{h,n} - u_h\right|^2_{H^1(\Omega_i)}. \tag{50}$$

Theorem 6.1. *If $\ell_{ov} \geq 0$ is sufficiently large, then*

$$\mathcal{E}_{h,n+1} \leq \theta \mathcal{E}_{h,n} \leq \theta^{n+1} \mathcal{E}_{h,0}, \quad n \geq 0,$$

where $\theta < 1$.

The contraction factor $\theta < 1$ is exponentially small in the number of mesh layers ℓ_{ov} of the overlap. Thus, even a modest overlap typically guarantees rapid convergence, while larger overlaps further improve the contraction.

Proof of Theorem 6.1. We define the differences $d^i_{h,n} = u^i_{h,n} - u_h\big|_{\Omega^i}$, for $i = 1, 2$, of the domain decomposition solution (48) and the global finite element solution (49). Combining the defintions of (48) and (49) shows that the differences solve the

problems

$$
\begin{aligned}
a_{\Omega_1}(d^1_{h,n+1}, \varphi^1_h) &= 0, \quad \text{for all } \varphi^1_h \in \mathcal{P}_{k,0}(\mathcal{T}_h(\Omega_1)) \\
d^1_{h,n+1}\Big|_{\Gamma_1} &= d^2_{h,n}\Big|_{\Gamma_1}, \\
a_{\Omega_2}(d^2_{h,n+1}, \varphi^2_h) &= 0, \quad \text{for all } \varphi^1_h \in \mathcal{P}_{k,0}(\mathcal{T}_h(\Omega_2)) \\
d^2_{h,n+1}\Big|_{\Gamma_2} &= d^1_{h,n}\Big|_{\Gamma_2},
\end{aligned} \tag{51}
$$

for $n \geq 0$.

We note that any discrete lifting, which is a projection on the discrete trace space $\mathcal{P}_k(\mathcal{T}_h(\Omega_i))\big|_{\Gamma^i} \cap H^{1/2}_{00}(\Gamma_i)$, produces the same sequence of solutions, since the associated bilinearforms are coercive and hence, the solution is unique. In order to use a sharp a-priori bound of the discrete solution, we choose a localized lifting. We fix a localization parameter $\epsilon > 0$ independent of h and choose liftings $d^i_{h,\epsilon,n+1} \in \mathcal{P}_k(\mathcal{T}_h(\Omega_i)) \cap H^1_{\partial\Omega_i \setminus \Gamma_i}(\Omega_i)$ such that

$$
d^1_{h,\epsilon,n+1}\Big|_{\Gamma_1} = d^2_{h,n}\Big|_{\Gamma_1}, \qquad d^2_{h,\epsilon,n+1}\Big|_{\Gamma_2} = d^1_{h,n}\Big|_{\Gamma_2},
$$

with

$$
\operatorname{supp} d_{h,\epsilon,n+1} \subset \Omega_{i,\epsilon} = \{\, x \in \Omega_i \mid \operatorname{dist}(x, \Gamma_i) \leq \epsilon \,\}.
$$

A suitable lifting is constructed in Appendix A, which is based on a Scott-Zhang interpolation operator together with a localization argument. In Corollary A.2, we prove the bounds

$$
\begin{aligned}
\|d^1_{h,\epsilon,n+1}\|_{H^1(\Omega_1)} &\leq C_1 \epsilon^{-1/2} \|d^2_{h,n}\|_{H^{1/2}_{00}(\Gamma_1)'} \\
\|d^2_{h,\epsilon,n+1}\|_{H^1(\Omega_2)} &\leq C_2 \epsilon^{-1/2} \|d^1_{h,n}\|_{H^{1/2}_{00}(\Gamma_2)'},
\end{aligned} \tag{52}
$$

with constants $C_1, C_2 > 0$ that only depend on the shape regularity of the mesh and not on h and ϵ.

Combining the definition of the discrete error (50), the a-prior estimate (11), and the inequalities (52), we obtain the estimate

$$
\begin{aligned}
\mathcal{E}_{h,n+1} &= \sum_{i=1,2} \left| u^i_{h,n+1} - u_h \right|^2_{H^1(\Omega_i)} = \sum_{i=1,2} \left| d^i_{h,n+1} \right|^2_{H^1(\Omega_i)} \\
&\leq 4 \Big(\left\| d^1_{h,\epsilon,n+1} \right\|^2_{H^1(\Omega_1)} + \left\| d^2_{h,\epsilon,n+1} \right\|^2_{H^1(\Omega_2)} \Big) \\
&\leq 4\epsilon^{-1} \Big(C_1^2 \left\| d^2_{h,n} \right\|^2_{H^{1/2}_{00}(\Gamma_1)} + C_2^2 \left\| d^1_{h,n} \right\|^2_{H^{1/2}_{00}(\Gamma_2)} \Big)
\end{aligned}
$$

The trace inequality now allows swapping from one subdomain Ω_j to its complement $\Omega \setminus \Omega_i$, that is

$$
\|d^j_{h,n}\|^2_{H^{1/2}_{00}(\Gamma_i)} = \|u^j_{h,n} - u_h\|^2_{H^{1/2}_{00}(\Gamma_i)} \leq C_{\mathrm{tr}} \left| u^j_{h,n} - u_h \right|^2_{H^1(\Omega \setminus \Omega_i)}, \quad i = 1,2, \text{ and } j \neq i.
$$

See also Figure 5 for an illustration. We now use the decay estimate of Theorem 3.1b) to enlarge the complementary domain to the full subdomain, gaining a contraction factor depending on the size of the overlap ℓ_{ov}. That is,

$$
\left| u^j_{h,n} - u_h \right|^2_{H^1(\Omega \setminus \Omega_i)} \leq \rho^{\ell_{\mathrm{ov}}} \left| u^j_{h,n} - u_h \right|^2_{H^1(\Omega_j)},
$$

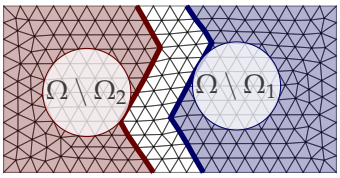

FIGURE 5. The complement domains $\Omega \setminus \Omega_i$ in the example decomposition of Figure 4. Note, that $\Omega \setminus \Omega_1 \subset \Omega_2$ and vice versa.

with $\rho = M_0/(1+M_0) < 1$ for $j = 1,2$ and $i \neq j$. Combining the previous estimates then yields

$$\mathcal{E}_{h,n+1} \leq \frac{4}{\epsilon} \max\{C_1^2, C_2^2\} C_{\mathrm{tr}} \rho^{\ell_{\mathrm{ov}}} \left(\left| u_{h,n}^1 - u_h \right|_{H^1(\Omega_1)}^2 + \left| u_{h,n}^2 - u_h \right|_{H^1(\Omega_2)}^2 \right) = C \rho^{\ell_{\mathrm{ov}}} \mathcal{E}_{h,n}.$$

Hence, if ℓ_{ov} is sufficiently large such that

$$\theta := 4\epsilon^{-1} \max\{C_1^2, C_2^2\} C_{\mathrm{tr}}\, \rho^{\ell_{\mathrm{ov}}} < 1,$$

the method converges independently of the initial iterates $u_{h,0}^1$ and $u_{h,0}^2$, which proves the claim. □

7. NUMERICAL VALIDATION

In this section, we numerically validate the discrete energy decay proven in Section 3, namely

$$E_{D_h}(\ell) \leq \rho E_{D_h}(\ell+1), \quad \ell < \ell_{\max},$$

where $\rho < 1$ denotes the contraction factor from Corollary 3.2 and the discrete energy $E_{D_h}(\ell)$ is defined in (16). Moreover, we compare the observed decay rates with the asymptotic scaling predicted by the estimate in Corollary 3.3.

For each numerical example, we consider a domain Ω equipped with a conforming triangulation $\mathcal{T}_h(\Omega)$ and fix the polynomial degree k of the finite element discretization. On $\Gamma \subseteq \partial\Omega$, we impose inhomogeneous Dirichlet boundary data g, while homogeneous Dirichlet conditions are prescribed on the complementary part Γ^C. Furthermore, we specify a starting patch $D_h \subset \mathcal{T}_h = \mathcal{T}_h(\Omega)$. Throughout this section we denote the discrete solution by

$$u_h = u_{h0} + u_{hg} \in \mathcal{P}_k(\mathcal{T}_h),$$

where u_{h0} denotes the solution of (10).

Measurement of the contraction factor ρ. The total energy of the discrete solution u_h on Ω is given by $|||u_h|||_\Omega^2$, cf. (5). For each layer $\ell = 0, \ldots, \ell_{\max}$, we construct the corresponding patch $\mathcal{P}_\ell(D_h)$ and compute the localized energy $E_{D_h}(\ell)$ according to (16). For comparability, we introduce the relative energy

$$E_{D_h}^{\mathrm{rel}}(\ell) := \frac{E_{D_h}(\ell)}{|||u_h|||_\Omega^2}, \quad \text{for } 0 \leq \ell \leq \ell_{\max}. \tag{53}$$

A semilogarithmic plot of the values $E_{D_h}^{\mathrm{rel}}(\ell)$ already provides a first indication of the expected exponential decay.

To determine the contraction factor quantitatively, we form the quotient

$$Q_{D_h}(\ell) = \frac{E_{D_h}^{\mathrm{rel}}(\ell)}{E_{D_h}^{\mathrm{rel}}(\ell+1)}, \quad \text{for } 0 \leq \ell < \ell_{\max}.$$

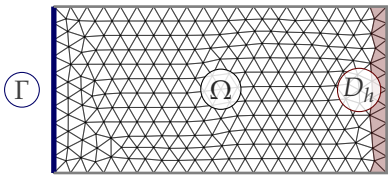

FIGURE 6. Triangular finite element mesh of the rectangular domain Ω with inhomogeneous boundary conditions prescribed on Γ (left boundary). The initial cell set D_h is highlighted in red. The displayed mesh corresponds to target mesh size $h_{\text{tar}} = 0.1$. Simulations were performed on independently generated finer meshes.

For a fixed layer ℓ, this quotient measures the ratio of the energy contained in the patch $P_\ell(D_h)$ to that of the next larger patch. Equivalently, it represents the local slope of the relative energy increase from layer ℓ to layer $\ell + 1$.

In practice, the values of $Q_{D_h}(\ell)$ may exhibit mild fluctuations for the first and the last few layers. In our experiments, we observed slightly smaller quotients for small ℓ, while the quotients tend to increase for large ℓ as the patches approach the full domain Ω. To obtain a single representative value of the contraction factor for a given configuration, we therefore define $\widehat{\rho}$ as the median of the set $\{Q_{D_h}(\ell)\}_{0\le\ell<\ell_{\max}}$, i.e.,

$$\widehat{\rho} := \text{median}\{\, Q_{D_h}(\ell) \mid 0 \le \ell < \ell_{\max} \,\}. \tag{54}$$

This quantity provides a robust estimate of the slope of the normalized energies for the majority of layers as verified later.

7.1. **Rectangular domain with inhomogeneous boundary conditions on the left.** As a first numerical example, we consider the rectangular domain

$$\Omega = [0, 2] \times [0, 1],$$

with boundary decomposition $\partial\Omega = \Gamma \cup \Gamma^C$, where

$$\Gamma = \partial\Omega \cap \{(x, y) \in \mathbb{R}^2 : x = 0\}.$$

The domain is discretized by a non-equidistant triangulation $\mathcal{T}_h = \mathcal{T}_h(\Omega)$ generated using gmsh (cf. [15]), and we employ linear finite elements. The resulting mesh with target mesh size $h_{\text{tar}} = 0.1$ is shown in Figure 6, with $h_{\min} \approx 0.089$ and $h = h_{\max} \approx 0.117$. For the later experiments, finer meshes were generated using smaller values of h_{tar}.

On $\Gamma \subseteq \partial\Omega$ we prescribe the inhomogeneous Dirichlet datum

$$g(y) = \sin(\pi y).$$

We first verify that the proposed procedure for measuring the contraction factor $\widehat{\rho}$ is justified; see Figures 7 and 8, where we depict the relative energies $E^{\text{rel}}_{D_h}(\ell)$ and the per-layer quotients $Q_{D_h}(\ell)$, respectively. Moreover, the data exhibit extremely low dispersion around the median, which is quantified by the median absolute deviation (MAD), which is defined as

$$\text{MAD} := \text{median}\{\, \left|Q_{D_h}(\ell) - \widehat{\rho}\right| \mid 0 \le \ell < \ell_{\max} \,\}$$

and reported in Table 1.

The small MAD values (of order 10^{-5}) indicate that the layer-wise quotients $Q_{D_h}(\ell)$ exhibit only negligible fluctuations around their median, apart from the first few layers. This quantitatively confirms the strong alignment observed in

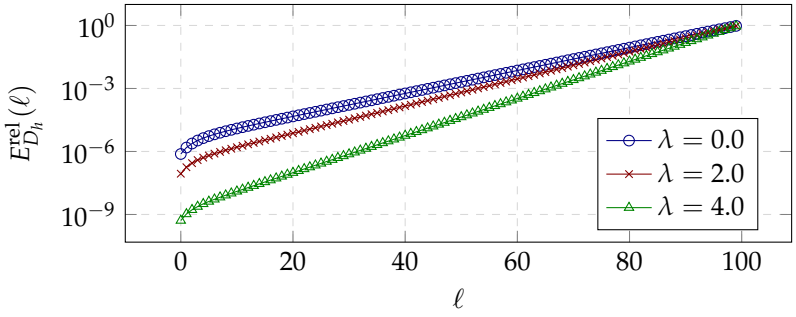

FIGURE 7. Relative energy $E^{\mathrm{rel}}_{D_h}(\ell)$ on the patches $P_\ell(D_h)$ for $0 \leq \ell \leq \ell_{\max}$ shown in a semilogarithmic plot for different values of λ. The approximately linear behavior indicates exponential growth with respect to ℓ. The underlying mesh was generated with target mesh size $h_{tar} = 0.02$.

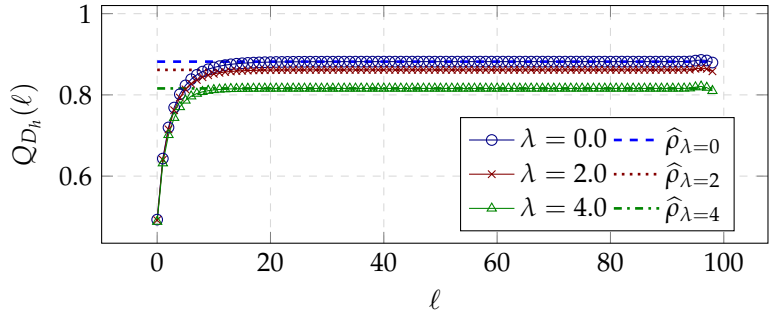

FIGURE 8. Layer-wise quotients of relative energies $Q_{D_h}(\ell)$ for $0 \leq \ell < \ell_{\max}$ and different values of λ (solid lines). The horizontal dashed, dotted, and dash-dotted lines indicate the corresponding median values $\widehat{\rho}$. The underlying mesh was generated with target mesh size $h_{\mathrm{tar}} = 0.02$.

	$\widehat{\rho}$	MAD
$\lambda = 0.0$	0.882	$4.44 \cdot 10^{-05}$
$\lambda = 2.0$	0.862	$4.33 \cdot 10^{-05}$
$\lambda = 4.0$	0.816	$2.65 \cdot 10^{-05}$

TABLE 1. Median contraction factor $\widehat{\rho}$ and MAD of the layer-wise quotients $Q_{D_h}(\ell)$ for different values of λ. The MAD quantifies the typical deviation of the quotients from their median.

Figure 8 and supports the interpretation of $\widehat{\rho}$ as a robust representative contraction factor.

Next, our goal is to investigate the dependence of the measured contraction factor $\widehat{\rho}$ on the mesh size h. To this end, we perform a sequence of computations on successively refined meshes; see Figure 9.

The numerical results indicate that the decay factor per layer approaches 1 as $h \to 0$. At first glance, this behavior appears to contradict the discrete decay result. However, this effect can be explained by the fact that both the diameter of the

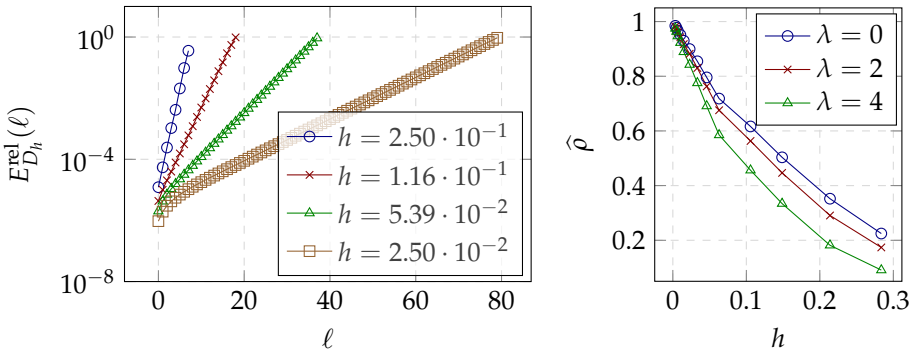

FIGURE 9. Left: Relative energies $E^{\mathrm{rel}}_{D_h}(\ell)$ in a semilogarithmic plot versus the layer index ℓ for $\lambda = 0$ and different mesh sizes h. Right: Measured contraction factor $\widehat{\rho}$ plotted against h for different values of λ.

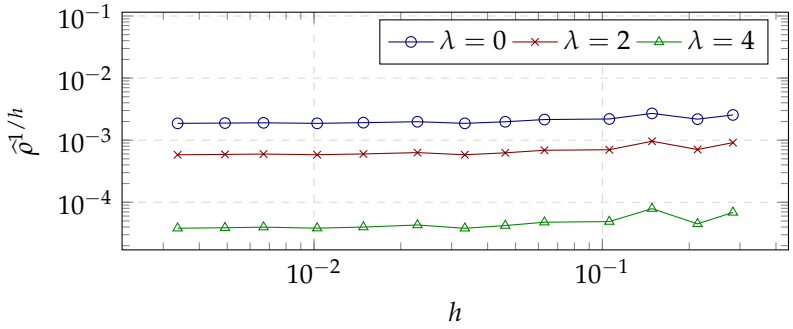

FIGURE 10. Scaled contraction factor $\widehat{\rho}^{1/h}$ plotted against the mesh size h in a double logarithmic scale for different values of λ. As $h \to 0$, the scaled contraction factor approaches a constant, in agreement with the asymptotic prediction of Corollary 3.3.

starting patch D_h and the physical width of each layer Σ_ℓ decrease with h. At the same time, the maximal layer index $\ell_{\max}$ increases as the mesh is refined, so that the discrete Saint-Venant principle from Theorem 3.1 can be applied over a larger number of layers.

Motivated by the asymptotic estimate in Corollary 3.3, we therefore rescale the measured decay by raising the data to the power $1/h$. The resulting behavior is shown in Figure 10 and we see that the scaled rate indeed behaves like a constant, when $h \to 0$.

7.2. **Hexagonal domain with inhomogeneous boundary conditions on all sides.** We consider a hexagonal domain centered at the origin, where the distance from each vertex to the origin is equal to one. On the entire boundary $\Gamma = \partial\Omega$, we prescribe the inhomogeneous Dirichlet condition $g \equiv 1$. The mesh is constructed such that it contains a structured submesh covering the square $[-0.2, 0.2] \times [-0.2, 0.2]$, see Figure 11. The starting patch D_h is chosen as the collection of all elements $K \in \mathcal{T}_h$ belonging to this embedded submesh. By this construction, the geometric support $\bigcup_{K \in D_h} \overline{K}$ remains of fixed physical size under mesh refinement.

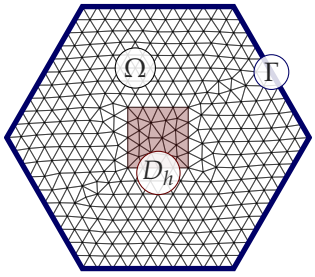

FIGURE 11. Triangular finite element mesh of the hexagonal domain Ω with inhomogeneous Dirichlet boundary condition $g \equiv 1$ prescribed on $\Gamma = \partial\Omega$. The starting patch D_h (red) consists of the elements of the structured submesh covering the square $[-0.2, 0.2]^2$. The depicted mesh corresponds to target mesh size $h_{\text{tar}} = 0.1$.

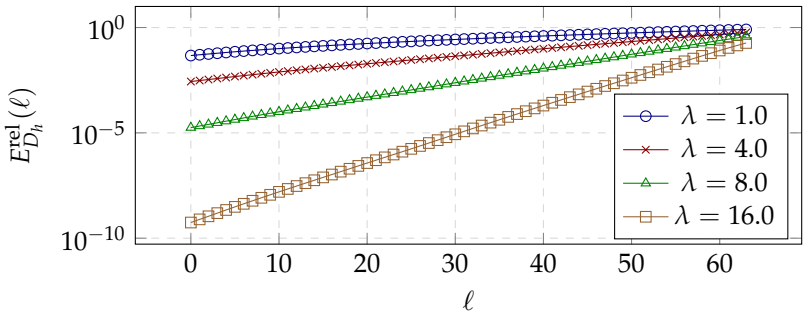

FIGURE 12. Relative energies $E^{\text{rel}}_{D_h}(\ell)$ plotted against the layer index ℓ in a semilogarithmic scale for different values of λ. The starting patch D_h has fixed physical support. The underlying mesh corresponds to target mesh size $h_{\text{tar}} = 0.01$.

In Figure 12, we plot the relative energies $E^{\text{rel}}_{D_h}(\ell)$ for a fixed mesh size h and all layers $0 \leq \ell < \ell_{\max}$, considering several values of the parameter λ. The approximately linear behavior confirms exponential decay per layer. The corresponding quotients $Q_{D_h}(\ell)$ are shown in Figure 13, where we additionally indicate the median value $\widehat{\rho}$ for each choice of λ.

Overall, the measurement $\widehat{\rho}$ still provides a reasonable characterization of the decay behavior, in particular for larger values of λ. For small λ, however, the median quotient may be pessimistic in the sense that the decay in the first few layers is even stronger than suggested by $\widehat{\rho}$; see Figures 12 and 13.

Rather than rescaling the median quotient by a power of $1/h$, we therefore adopt the more geometric point of view discussed in Remark 3.4. Motivated by the fixed physical size of the initial patch $D_h = P_0(D_h)$, we introduce a layer index $\ell^\star = \ell^\star(h)$ such that the enlarged patch $P_{\ell^\star}(D_h)$ covers a neighborhood of D_h with fixed physical width. More precisely, we fix a parameter $\delta := \ell^\star h_{\min}$, where $h_{\min}$ denotes the minimal element diameter, so that δ represents the additional physical width of the patch $P_{\ell^\star}(D_h)$ compared to the initial cell set D_h.

In analogy with the asymptotic estimate in Corollary 3.3, we therefore expect the ratio of energies on D_h and $P_{\ell^\star}(D_h)$ to remain bounded as $h \to 0$.

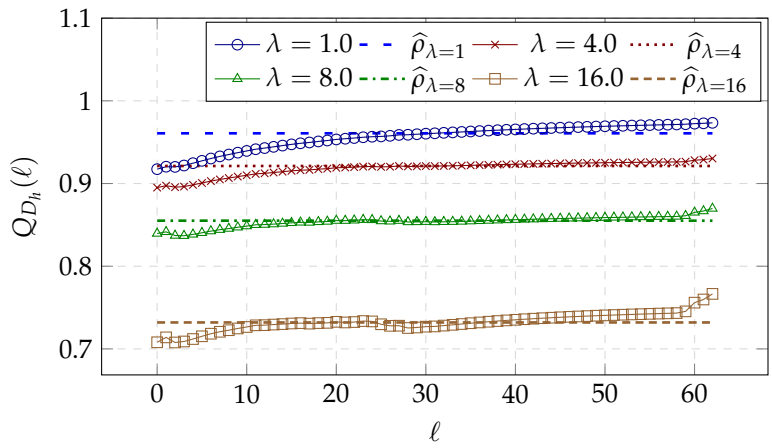

FIGURE 13. Layer-wise quotients $Q_{D_h}(\ell)$ for $0 \leq \ell < \ell_{\max}$ and different values of λ (solid lines). The horizontal dashed lines indicate the corresponding median contraction factors $\widehat{\rho}_\lambda$. The starting patch D_h has fixed physical support. Mesh target size $h_{\text{tar}} = 0.01$.

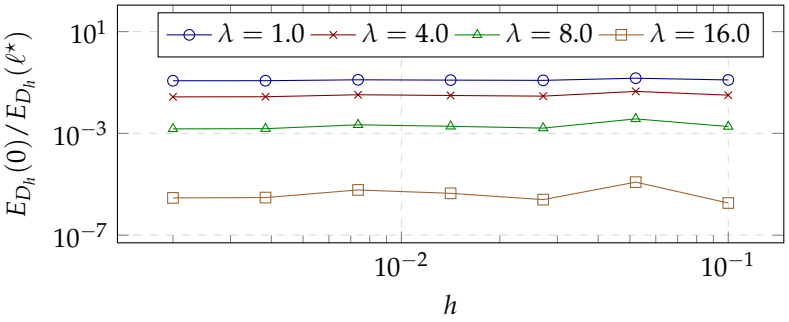

FIGURE 14. Energy ratio $E_{D_h}(0)/E_{D_h}(\ell^\star)$ plotted against the mesh size h for fixed physical width $\delta = \ell^\star h_{\min} = 0.3$ and different values of λ. The near constant behavior as $h \to 0$ confirms the exponential decay with respect to physical distance as stated in Corollary 3.3.

To verify this, we plot the energy ratio $E_{D_h}(0)/E_{D_h}(\ell^\star)$ against h for a fixed value $\delta \equiv 0.3$; see Figure 14. Finally, Figure 15 shows that the logarithm of this ratio depends linearly (with negative slope) on λ, in full agreement with the predicted structure of the constant in Corollary 3.3.

Conclusion. The numerical experiments fully confirm the discrete Saint-Venant principle and its asymptotic interpretation. The relative energies exhibit a clear exponential decay with respect to the layer index, and the layer-wise quotients remain remarkably stable, as quantified by the small median absolute deviations. Under mesh refinement, the measured contraction factor behaves consistently with the predicted scaling, approaching unity per layer while yielding a constant decay rate per physical distance. In the fixed-width setting, the energy drop across a prescribed physical neighborhood remains bounded as $h \to 0$, and its logarithm

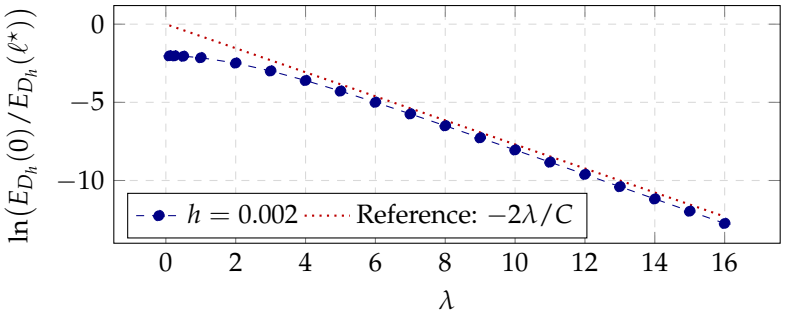

FIGURE 15. Dependence of $\ln\big(E_{D_h}(0)/E_{D_h}(\ell^\star)\big)$ on λ for $h_{\text{tar}} = 0.002$. The dotted line shows the reference slope $-2\lambda/C$ with $C = 2.6$, in accordance with Corollary 3.3. The linear behavior confirms the predicted exponential dependence of the decay rate on λ.

depends linearly on λ, in precise agreement with the structure predicted by Corollary 3.3. Together, these results provide comprehensive numerical validation of the theoretical decay estimates.

The code accompanying the numerical experiments is publicly available at

https://gitlab.kit.edu/tim.buchholz/dsv-numerical-validation.git .

APPENDIX A. LOCAL BOUNDARY LIFTING

We are in the setting of Section 2.2, i.e., $\Omega \subset \mathbb{R}^d$ is a polyhedral domain and $\Gamma \subset \partial\Omega$ a simply connected subset of the boundary with complement $\Gamma^{\mathrm{C}} = \partial\Omega \setminus \Gamma$. In this section, we assume that $\Gamma \neq \emptyset$ and restrict ourselves to $d = 2$ for the sake of presentation.

The aim of this section is to construct a discrete lifting for $g \in H^{1/2}_{00}(\Gamma)$, that is H^1-stable and localized in an ϵ-neighborhood of Γ. We use a common construction by interpolating a harmonic extension of the trace on the strip. Since we demand that the lifting is a projection with respect to $\mathcal{P}_k(\mathcal{T}_h)|_\Gamma$, we use the Scott-Zhang quasi-interpolation [35], which is precisely constructed for that purpose. Furthermore, we explicitly track the thickness ϵ of the strip.

For a given geometry dependent $\epsilon_0 > 0$, we define for all $\epsilon \in (0, \epsilon_0)$ the tubular subdomain

$$\Omega_\epsilon = \{\, x \in \Omega \mid \operatorname{dist}(x, \Gamma) \leq \epsilon \,\} \subsetneq \Omega. \tag{55}$$

Note that a small enough ϵ_0 ensures that $\partial\Omega_\epsilon \setminus \Gamma$ is an offset of straight-line segments connected with circular arcs of radius ϵ for every vertex of Γ. Hence, Ω_ϵ is a Lipschitz domain.

Lemma A.1. *Let $g \in H^{1/2}_{00}(\Gamma)$ and $u_\epsilon \in H^1(\Omega_\epsilon)$ denote the harmonic extension, i.e.,*

$$-\Delta u_\epsilon = 0, \qquad u_\epsilon|_\Gamma = g, \qquad u_\epsilon|_{\partial\Omega_\epsilon \setminus \Gamma} = 0. \tag{56}$$

There exists a constant $C > 0$ independent of ϵ and g such that

$$\|u_\epsilon\|_{H^1(\Omega_\epsilon)} \leq C\epsilon^{-1/2} \|g\|_{H^{1/2}_{00}(\Gamma)}. \tag{57}$$

The Lemma is proved at the end of this section. We motivate the scaling $\epsilon^{-1/2}$ in dimension one. Let $\Omega = [0, 1]$ and $\Gamma = \{0\}$. Then, the solution of (56) for $g \in \mathbb{R}$ is

given by $u(x) = g(1 - \epsilon^{-1}x)$. Hence, we obtain the scaling $\|u'\|_{L^2(\Omega_\epsilon)} = \epsilon^{-1/2}|g|$, which is sharp in one dimension.

With Lemma A.1 and the Scott-Zhang interpolation operator in [35], we can proof the existence of the desired discrete lifting.

Corollary A.2. *Let $2h \leq \epsilon$. For $g \in H^{1/2}_{00}(\Gamma)$ there exists a discrete lifting $u_{hg} \in \mathcal{P}_k(\mathcal{T}_h) \cap H^1_{\Gamma^C}(\Omega)$ such that*

$$\left\|u_{hg}\right\|_{H^1(\Omega)} \leq C\epsilon^{-1/2} \|g\|_{H^{1/2}_{00}(\Gamma)}, \qquad \operatorname{supp} u_{hg} \subset \Omega_\epsilon,$$

where the constant $C > 0$ is independent of ϵ, g and h, but depends on the shape-regularity. For $g \in \mathcal{P}_k(\mathcal{T}_h)|_\Gamma \cap H^{1/2}_{00}(\Gamma)$ the lifting is a projection, i.e., $u_{hg}\big|_\Gamma = g$.

Note that $2h \leq \epsilon$ is not a restriction, since it only prohibits degenerate cases where the mesh size is too large to make sense of the claim $\operatorname{supp} u_{hg} \subset \Omega_\epsilon$.

Proof of Corollary A.2. Let $\epsilon' = \epsilon/2$ and define $u_{\epsilon'} \in H^1(\Omega_{\epsilon'})$ according to Lemma A.1. Since it holds $u_{\epsilon'}|_{\partial\Omega_{\epsilon'}\setminus\Gamma} = 0$, we can extend by zero to the whole of the domain Ω. We denote this extension with $\widetilde{u}_{\epsilon'} \in H^1_\Gamma(\Omega)$, satisfying the estimate

$$\|\widetilde{u}_{\epsilon'}\|_{H^1(\Omega)} = \|u_{\epsilon'}\|_{H^1(\Omega_{\epsilon'})} \leq C\sqrt{2}\epsilon^{-1/2} \|g\|_{H^{1/2}_{00}(\Gamma)}, \qquad \operatorname{supp} \widetilde{u}_{\epsilon'} \subset \Omega_{\epsilon'}.$$

Furthermore, let $\Pi^{\mathrm{SZ}}_h : H^1(\Omega) \to \mathcal{P}_k(\mathcal{T}_h)$ denote the Scott-Zhang interpolation operator, defined in [35, Sec. 2]. Then, the discrete lifting defined as $u_{hg} = \Pi^{\mathrm{SZ}}_h \widetilde{u}_{\epsilon'}$ fulfills the requirements.

With the stability in [35, Thm. 3.1] and Lemma A.1 it holds that

$$\left\|u_{hg}\right\|_{H^1(\Omega)} = \left\|\Pi^{\mathrm{SZ}}_h \widetilde{u}_{\epsilon'}\right\|_{H^1(\Omega)} \leq C \|\widetilde{u}_{\epsilon'}\|_{H^1(\Omega)} \leq C\sqrt{2}\epsilon^{-1/2} \|g\|_{H^{1/2}_{00}(\Gamma)}.$$

The discrete lifting is locally supported on Ω_ϵ since for any $K \in \mathcal{T}_h$ the value of the interpolation $u_{hg}\big|_K$ is completely controlled by its surrounding patch. Additionally, it fulfills the desired properties on the boundary, as mentioned in [35, Sec. 5]. □

It remains to prove Lemma A.1.

Proof of Lemma A.1. Note that the extension by zero $\widetilde{g} \in L^2(\partial\Omega_\epsilon)$ is an element of $H^{1/2}(\partial\Omega_\epsilon)$ since $g \in H^{1/2}_{00}(\Gamma)$ by assumption. Hence, since Ω_ϵ is Lipschitz, the Lax-Milgram Lemma ensures that a unique weak solution $u_\epsilon \in H^1(\Omega_\epsilon)$ exists. Furthermore, by the Dirichlet principle, u_ϵ is the minimizer of the functional

$$J : V_{\widetilde{g}} \to \mathbb{R}, \quad \phi \mapsto \frac{1}{2}\int_{\Omega_\epsilon} |\nabla\phi(x)|^2 \,\mathrm{d}x, \qquad V_{\widetilde{g}} = \{\, \phi \in H^1(\Omega_\epsilon) \mid \phi|_{\partial\Omega_\epsilon} = \widetilde{g} \,\}.$$

Thus, by the minimizing property and Poincaré inequality, it is sufficient to construct

$$v \in V_{\widetilde{g}}, \qquad \text{s.t. } \|v\|_{H^1(\Omega_\epsilon)} \leq C\epsilon^{-1/2} \|g\|_{H^{1/2}_{00}(\Gamma)}$$

in order to show (57). In the following, we construct such a suitable v with respect to a finite open cover of Γ, following essentially ideas from [19].

Let $V_\Gamma = \{\alpha_1, \dots \alpha_N\} \subset \mathbb{R}^2$ denote the vertices of Γ. For every vertex we define

$$U_j = B_\epsilon(\alpha_j) = \{\, x \in \mathbb{R}^2 \mid |x - \alpha_j| < \epsilon \,\}, \qquad j = 1, \dots, N.$$

Note that we can always choose $\epsilon_0 > 0$ in (55) sufficiently small such that for all $\epsilon \in (0, \epsilon_0)$ the set $U_j \cap \Omega$ contains no vertex α_k with $k \neq j$, and no edge except for the two edges adjacent to α_j.

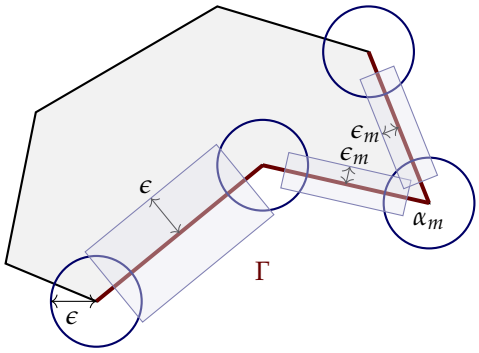

FIGURE 16. Finite cover of the boundary Γ for given $\epsilon > 0$. Note that $\epsilon_m < \epsilon$ due to the small interior angle at the vertex α_m.

The N vertices are connected by $N-1$ straight line elements, and can each be covered by a tubular neighborhood V_m of size $\epsilon_m > 0$, for $m = 1, \dots, N-1$, such that $V_m \cap \Omega$ does not contain any vertex and any other line element, but overlaps with the balls at the neighboring vertices. Note, that we need $\epsilon_m \leq \epsilon$ in general to accomplish this construction. Nonetheless, the additional restrictions on ϵ_m only depend on the angles of adjacent edges. Hence, there exists a $C > 0$ depending only on the smallest interior angle of the domain such that

$$\max_{m=1,\dots,N-1} \epsilon_m^{-1} \leq C\epsilon^{-1}, \tag{58}$$

see also Fig. 16.

Thus, the two sets $\{U_j\}_{j=1}^N$ and $\{V_j\}_{j=1}^{N-1}$ are an open cover of Γ, and we stress that N does not depend on ϵ but only on the number of vertices.

We choose a partition of unity subordinate to the cover, i.e., $\phi_j, \psi_m \in C_c^\infty(\mathbb{R}^2)$ such that

$$1 = \sum_{j=1}^{N} \phi_j(x) + \sum_{m=1}^{N-1} \psi_m(x), \quad x \in \Gamma, \qquad \operatorname{supp} \phi_j \subset U_j, \quad \operatorname{supp} \psi_m \subset V_m. \tag{59}$$

Next, we construct a local lifting in every corner. Let $j \in \{1, \dots, N\}$. We define the cone $K_j = \Omega \cap U_j$ of radius ϵ at the corner α_j and set $g_j = \phi_j g$. We denote the legs of K_j with $\Gamma_j = \overline{K_j} \cap \Gamma$ and the arc with A_j, forming the boundary of K_j. Note, that the support of ϕ_j is compact in U_j and, thus, the zero extension of g_j to ∂K_j is element of $H^{1/2}(\partial K_j)$. Hence, we conclude that there exists a unique $v_j \in H^1(K_j)$ solving

$$-\Delta v_j = 0, \text{ in } K_j, \qquad v_j\big|_{\Gamma_j} = g_j, \text{ on } \Gamma_j, \qquad v_j\big|_{A_j} = 0, \text{ on } A_j. \tag{60}$$

We prove the desired norm estimate with a scaling argument. After possible rigid motion, we can assume that the cone has the polar-coordinate representation

$$K_j = \{\, (r, \theta) \in \mathbb{R}^+ \times [0, 2\pi] \mid 0 < r < \epsilon, \quad \theta \in (0, \varphi) \,\},$$

for some angle $\varphi \in (0, 2\pi)$.

Let $\widehat{K} = \{\, (r, \theta) \in \mathbb{R}^+ \times [0, 2\pi] \mid 0 < r < 1, \quad \theta \in (0, \varphi) \,\}$ denote the reference cone with angle φ, and let $T : \widehat{K} \to K_j$ be the reference map given in Cartesian coordinates by $(x, y) \mapsto (rx, ry)$. Then, the transformed function $\widehat{v} = v_j \circ T$ solves

$$-\Delta \widehat{v} = 0, \text{ in } \widehat{K}, \qquad \widehat{v}|_{\widehat{\Gamma}} = \widehat{g}, \text{ on } \widehat{\Gamma}, \qquad \widehat{v}|_{\widehat{A}} = 0, \text{ on } \widehat{A},$$

where $\widehat{g} = g_j \circ T$, $\widehat{\Gamma} = T^{-1}(\Gamma_j)$, and $\widehat{A} = T^{-1}(A_j)$. With the usual a priori estimate and the Poincaré inequality, we obtain the estimate $\|\nabla \widehat{v}\|_{L^2(\widehat{K})} \lesssim \|\widehat{g}\|_{H^{1/2}_{00}(\widehat{\Gamma})}$, where the hidden constant only depends on the angle φ but not on the radius ϵ. From integral substitution, we further see that $\|\nabla v_j\|_{L^2(K_j)} = \|\nabla \widehat{v}\|_{L^2(\widehat{K})}$. Furthermore, it holds that

$$\begin{aligned} \|\widehat{g}\|^2_{L^2(\widehat{\Gamma})} &= \int_0^1 |(g_j \circ T)(r,0)|^2 + |(g_j \circ T)(r,\varphi)|^2 \,\mathrm{d}r \\ &= \int_0^1 |g_j(\epsilon r, 0)|^2 + |g_j(\epsilon r, \varphi)|^2 \,\mathrm{d}r \\ &= \epsilon^{-1} \int_0^\epsilon |g_j(\widetilde{r}, 0)|^2 + |g_j(\widetilde{r}, \varphi)|^2 \,\mathrm{d}\widetilde{r} \\ &= \epsilon^{-1} \|g_j\|^2_{L^2(\Gamma_j)}. \end{aligned} \tag{61}$$

For the semi-norm $|\cdot|_{H^{1/2}(\widehat{\Gamma})}$, let $\eta, \zeta \in \{0, \varphi\}$. With integral substitution, it holds that

$$\begin{aligned} &\int_0^1 \int_0^1 \frac{\left|(g_j \circ T)(r,\eta) - (g_j \circ T)(s,\zeta)\right|^2}{|r-s|^2} \,\mathrm{d}r \,\mathrm{d}s \\ &= \int_0^1 \int_0^1 \frac{\left|g_j(\epsilon r, \eta) - g_j(\epsilon s, \zeta)\right|^2}{|r-s|^2} \,\mathrm{d}r \,\mathrm{d}s \\ &= \int_0^\epsilon \int_0^\epsilon \frac{\left|g_j(\widetilde{r}, \eta) - g_j(\widetilde{s}, \zeta)\right|^2}{|\epsilon^{-1}\widetilde{r} - \epsilon^{-1}\widetilde{s}|^2} \epsilon^{-2} \,\mathrm{d}\widetilde{r} \,\mathrm{d}\widetilde{s} \\ &= \int_0^\epsilon \int_0^\epsilon \frac{\left|g_j(\widetilde{r}, \eta) - g_j(\widetilde{s}, \zeta)\right|^2}{|\widetilde{r} - \widetilde{s}|^2} \,\mathrm{d}\widetilde{r} \,\mathrm{d}\widetilde{s}. \end{aligned} \tag{62}$$

With the considerations in [19, Sec. 1.5.2], this shows that $|\widehat{g}|_{H^{1/2}(\widehat{\Gamma})} = |g_j|_{H^{1/2}(\Gamma_j)}$. Repeating the substitution argument for the compatibility conditions, which we can express as weighted L^2 integrals, shows that

$$\int_0^1 |1-r|^{-1} |(g_j \circ T)(r,\eta)|^2 \,\mathrm{d}r = \int_0^\epsilon |\epsilon - \widetilde{r}|^{-1} |g_j(\widetilde{r}, \eta)|^2 \,\mathrm{d}\widetilde{r}. \tag{63}$$

Thus, (61)–(63) show that $\|\widehat{g}\|_{H^{1/2}_{00}(\widehat{\Gamma})} \leq \epsilon^{-1/2} \|g_j\|_{H^{1/2}_{00}(\Gamma_j)}$. Hence, we conclude that

$$\|\nabla v_j\|_{L^2(K_j)} = \|\nabla \widehat{v}\|_{L^2(\widehat{K})} \lesssim \|\widehat{g}\|_{H^{1/2}_{00}(\widehat{\Gamma})} \lesssim \epsilon^{-1/2} \|g_j\|_{H^{1/2}_{00}(\Gamma_j)}, \tag{64}$$

with the hidden constant only depending on the angle φ.

Next, we construct a lifting for every straight edge. Let $T_m = \Omega \cap V_m$ for $m \in \{0, \dots, N-1\}$. After possible rigid motion, we can assume that

$$T_m = (\delta_m^-, \delta_m^+) \times (0, \epsilon_m),$$

for $\delta_m^\pm > 0$. We define $\Gamma_m = (\delta_m^-, \delta_m^+) \times \{0\}$ and $g_m = \psi_m g$. Note that $g_m \in H^{1/2}_{00}(\Gamma_m)$ since ψ_m is compactly supported. Hence, there exists a unique $w_m \in H^1(T_m)$ solving

$$-\Delta w_m = 0, \text{ in } T_m, \quad w_m|_{\Gamma_m} = g_m, \text{ on } \Gamma_m, \quad w_m|_{\partial T_m \setminus \Gamma_m} = 0, \text{ on } \partial T_m \setminus \Gamma_m.$$

In order to prove an estimate like above on the cone, we use an explicit representation of the solution. Since $g_m \in H^{1/2}_{00}(\Gamma_m)$, we find a sine series expansion of

the data

$$g_m(x) = \sum_{n=1}^{\infty} g_m^n \sin\Big(\frac{\pi n}{L}(x-\delta^-)\Big),$$

where $L = (\delta^+ - \delta^-)$ and $g_m^n = \frac{2}{L}\int_{\delta^-}^{\delta^+} g_m(\zeta)\sin\Big(\frac{\pi n}{L}(\zeta-\delta^-)\Big)\,\mathrm{d}\zeta$, for $n \geq 1$. A separation of variables ansatz and matching this expansion at Γ_m $(y = 0)$ shows that the solution is of the form

$$w_m(x,y) = \sum_{n=1}^{\infty} g_m^n \frac{\sinh(k_n(\epsilon_m - y))}{\sinh(k_n\epsilon_m)}\sin(k_n(x-\delta^-)), \qquad k_n = \frac{n\pi}{L}.$$

Taking derivates and using standard orthogonality relations of trigonometric functions show that

$$\|\nabla w_m\|^2_{L^2(T_m)} = \frac{L}{2}\sum_{n=1}^{\infty}|g_m^n|^2 k_n^2 \int_0^{\epsilon_m} \frac{\sinh^2(k_n y) + \cosh^2(k_n y)}{\sinh^2(k_n\epsilon_m)}\,\mathrm{d}y.$$

To evaluate the latter integral, we use the identity $\sinh^2(k_n y) + \cosh^2(k_n y) = \cosh(2k_n y)$ and obtain

$$\frac{1}{\sinh^2(k_n\epsilon_m)}\int_0^{\epsilon_m}\cosh(2k_n y)\,\mathrm{d}y = \frac{1}{2k_n}\frac{\sinh(2k_n\epsilon_m)}{\sinh^2(k_n\epsilon_m)} = \frac{1}{2k_n}\coth(k_n\epsilon_m),$$

where the half-angle formula $\sinh(2k_n\epsilon_m) = 2\sinh(k_n\epsilon_m)\cosh(k_n\epsilon_m)$ is used in the last equality. Hence, we obtain the representation

$$\|\nabla w_m\|^2_{L^2(T_m)} = \frac{L}{4}\sum_{n=1}^{\infty}|g_m^n|^2 k_n \coth(k_n\epsilon_m).$$

Application of the estimate $\coth(k_n\epsilon_m) \leq 1 + (k_n\epsilon_m)^{-1}$ finally shows that

$$\|\nabla w_m\|_{L^2(T_m)} \leq \epsilon_m^{-1/2}\,\|g_m\|_{H^{1/2}_{00}(\Gamma_m)}. \tag{65}$$

Putting everything together, we define $v \in H^1(\Omega)$ by $v = \sum_{j=1}^{N} v_j + \sum_{m=1}^{N-1} w_m$. Note that v is well-defined since any v_j and any w_m can be extended by zero to the whole of the domain, while remaining in $H^1(\Omega)$ due to the homogenous Dirichlet boundary conditions at the interior boundary. Furthermore, by the partition of unity (59), we conclude that

$$v|_\Gamma = \sum_{j=1}^{N} v_j|_\Gamma + \sum_{m=1}^{N-1} w_m|_\Gamma = \sum_{j=1}^{N}\phi_j g + \sum_{m=1}^{N-1}\psi_m g = g.$$

Finally, by (64), (65), (58), and the fact that the partition is finite, we obtain the desired estimate

$$\|\nabla v\|_{L^2(\Omega)} \leq C\epsilon^{-1/2}\,\|g\|_{H^{1/2}_{00}(\Gamma)},$$

with a constant $C > 0$, which is independent of ϵ. This proves the claim. □

ACKNOWLEDGMENTS

Funded by the Deutsche Forschungsgemeinschaft (DFG, German Research Foundation) – Project-ID 258734477 – SFB 1173. The authors thank Benjamin Dörich and Roland Maier for many helpful discussions and careful reading of the manuscript. JD thanks the French Institute for Research in Computer Science and Automation (Inria) in Lille for the kind hospitality during his research stay. This research stay was financially supported by the Karlsruhe House of Young Scientists (KHYS).

REFERENCES

[1] C. Alber, C. Ma, and R. Scheichl, *A mixed multiscale spectral generalized finite element method*, Numer. Math. **157** (2025), no. 1, 1–40. MR4858130

[2] R. Altmann, P. Henning, and D. Peterseim, *Quantitative Anderson localization of Schrödinger eigenstates under disorder potentials*, Math. Models Methods Appl. Sci. **30** (2020), no. 5, 917–955. MR4098219

[3] S. C. Brenner and L. R. Scott, *The mathematical theory of finite element methods*, Third, Texts in Applied Mathematics, vol. 15, Springer, New York, 2008. MR2373954

[4] T. Buchholz and M. Hochbruck, *A non-iterative domain decomposition time integrator for linear wave equations*, Math. Comp. (2026). https://doi.org/10.1090/mcom/4234.

[5] P. G. Ciarlet, *The finite element method for elliptic problems*, Classics in Applied Mathematics, vol. 40, Society for Industrial and Applied Mathematics (SIAM), Philadelphia, PA, 2002. Reprint of the 1978 original [North-Holland, Amsterdam; MR0520174 (58 #25001)]. MR1930132

[6] X. Claeys and R. D. Atchekzai, *Accelerating non-local exchange in generalized optimized Schwarz methods*, SMAI J. Comput. Math. **11** (2025), 517–532. MR4967330

[7] X. Claeys and E. Parolin, *Robust treatment of cross-points in optimized Schwarz methods*, Numer. Math. **151** (2022), no. 2, 405–442. MR4433119

[8] A. Ern and JL. Guermond, *Finite elements I—Approximation and interpolation*, Texts in Applied Mathematics, vol. 72, Springer, Cham, 2021. MR4242224

[9] ———, *Finite elements II—Galerkin approximation, elliptic and mixed PDEs*, Texts in Applied Mathematics, vol. 73, Springer, Cham, 2021. MR4269305

[10] D. Gallistl and R. Maier, *Localized implicit time stepping for the wave equation*, SIAM J. Numer. Anal. **62** (2024), no. 4, 1589–1608. MR4772556

[11] M. J. Gander, *Analysis of parallel algorithms for time-dependent partial differential equations*, ProQuest LLC, Ann Arbor, MI, 1997. Thesis (Ph.D.)–Stanford University. MR2696586

[12] ———, *Schwarz methods over the course of time*, Electron. Trans. Numer. Anal. **31** (2008), 228–255. MR2569603

[13] M. J. Gander, SL. Wu, and T. Zhou, *Time parallelization for hyperbolic and parabolic problems*, Acta Numer. **34** (2025), 385–489. MR4926314

[14] M. J. Gander and H. Zhang, *Schwarz methods by domain truncation*, Acta Numer. **31** (2022), 1–134. MR4436585

[15] C. Geuzaine and JF. Remacle, *Gmsh: A 3-D finite element mesh generator with built-in pre- and post-processing facilities*, Internat. J. Numer. Methods Engrg. **79** (2009), no. 11, 1309–1331. MR2566786

[16] E. Giladi and H. B. Keller, *Space-time domain decomposition for parabolic problems*, Numer. Math. **93** (2002), no. 2, 279–313. MR1941398

[17] A. Gloria, *Reduction of the resonance error—Part 1: Approximation of homogenized coefficients*, Math. Models Methods Appl. Sci. **21** (2011), no. 8, 1601–1630. MR2826466

[18] J. Gopalakrishnan, J. Schöberl, and C. Wintersteiger, *Mapped tent pitching schemes for hyperbolic systems*, SIAM J. Sci. Comput. **39** (2017), no. 6, B1043–B1063. MR3725284

[19] P. Grisvard, *Elliptic problems in nonsmooth domains*, Classics in Applied Mathematics, vol. 69, Society for Industrial and Applied Mathematics (SIAM), Philadelphia, PA, 2011. Reprint of the 1985 original [MR0775683], With a foreword by Susanne C. Brenner. MR3396210

[20] C. O. Horgan, *Recent developments concerning Saint-Venant's principle: an update*, AMR **42** (1989), no. 11, 295–303. MR1021553

[21] ———, *Recent developments concerning saint-venant's principle: a second update*, AMR **48** (1996), 101–111.

[22] C. O. Horgan and J. K. Knowles, *Recent developments concerning Saint-Venant's principle*, Adv. in Appl. Mech. **23** (1983), 179–269. MR889288

[23] C. O. Horgan and L. T. Wheeler, *Exponential decay estimates for second-order quasi-linear elliptic equations*, J. Math. Anal. Appl. **59** (1977), no. 2, 267–277. MR509055

[24] R. B. Kellogg, *On the Poisson equation with intersecting interfaces*, Applicable Anal. **4** (1974/75), 101–129. MR393815

[25] J. K. Knowles, *On Saint-Venant's principle in the two-dimensional linear theory of elasticity*, Arch. Rational Mech. Anal. **21** (1966), 1–22. MR187480

[26] JL. Lions and E. Magenes, *Non-homogeneous boundary value problems and applications. Vol. I*, Die Grundlehren der mathematischen Wissenschaften, vol. Band 181, Springer-Verlag, New York-Heidelberg, 1972. Translated from the French by P. Kenneth. MR350177

[27] P.-L. Lions, *On the Schwarz alternating method. I*, First International Symposium on Domain Decomposition Methods for Partial Differential Equations (Paris, 1987), 1988, pp. 1–42. MR972510

[28] A. E. H. Love, *A treatise on the mathematical theory of elasticity*, 4th ed., Dover Publications, New York, 1944. MR10851

[29] C. Ma, R. Scheichl, and T. Dodwell, *Novel design and analysis of generalized finite element methods based on locally optimal spectral approximations*, SIAM J. Numer. Anal. **60** (2022), no. 1, 244–273. MR4372648
[30] A. Målqvist and D. Peterseim, *Localization of elliptic multiscale problems*, Math. Comp. **83** (2014), no. 290, 2583–2603. MR3246801
[31] ———, *Numerical homogenization by localized orthogonal decomposition*, SIAM Spotlights, vol. 5, Society for Industrial and Applied Mathematics (SIAM), Philadelphia, PA, 2021. MR4191211
[32] HJ. Mieth, *Über abklingende Lösungen elliptischer Randwertprobleme (Prinzip von Saint-Venant)*, Ph.D. Thesis, 1975.
[33] ———, *Ein Saint-Venantsches Prinzip für eine Klasse von modifizierten Dirichlet-Problemen*, Z. Angew. Math. Mech. **56** (1976), no. 3, T258–T260. MR450776
[34] A. J. C. B. Saint-Venant, *Mémoire sur la torsion des prismes et sur leur flexion ainsi que sur l'équilibre intérieur des solides élastiques en génénéral*, Mémoires présentés par divers savants à l'Académie des Sciences, Académie des sciences, Paris, 1856. Original memoir containing the Saint-Venant principle.
[35] L. R. Scott and S. Zhang, *Finite element interpolation of nonsmooth functions satisfying boundary conditions*, Math. Comp. **54** (1990), no. 190, 483–493. MR1011446
[36] A. Toselli and O. Widlund, *Domain decomposition methods—algorithms and theory*, Springer Series in Computational Mathematics, vol. 34, Springer-Verlag, Berlin, 2005. MR2104179
[37] R. A. Toupin, *Saint-Venant's principle*, Arch. Rational Mech. Anal. **18** (1965), 83–96. MR172506
[38] L. T. Wheeler and C. O. Horgan, *A two-dimensional Saint-Venant principle for second-order linear elliptic equations*, Quart. Appl. Math. **34** (1976/77), no. 3, 257–270. MR450770

T. BUCHHOLZ, J. DÖRNER
INSTITUTE FOR APPLIED AND NUMERICAL MATHEMATICS,
KARLSRUHE INSTITUTE OF TECHNOLOGY (KIT),
D-76128 KARLSRUHE, GERMANY
Email address: {tim.buchholz,julian.doerner}@kit.edu